scientific reports

Impact Factor 3.9
Q1

Check for updates

OPEN

Development and evaluation of S-carboxymethyl-L-cystine-loaded solid lipid nanoparticles for Parkinson's disease in murine and zebrafish models

Shannon D Almeida[1], Sameera Hammigi Ramesh[1], Govardhan Katta Radhakrishna[1], Golla Sireesha[2], Soundarya Ramesh[2], Bandral Sunil Kumar[2], Basavana Gowda Hosur Dinesh[2], Srinivas Ganjipete[2], Sunil Nagaraj[3], Panneerselvam Theivendren[4], Kumarappan Chidambaram[5], Selvaraj Kunjiappan[6]✉, Damodar Nayak Ammunje[1]✉ & Parasuraman Pavadai[2]✉

Parkinson's disease (PD) is an advanced neurodegenerative condition distinguished by the rapid decline of dopamine neurons in the midbrain, leading to an imbalance in dopamine and acetylcholine levels, precipitating associated symptoms. The main objective of this work was to fabricate solid lipid nanoparticles (SLNs) loaded with S-carboxymethyl-L-cystine (SC) for enhanced delivery to the brain. This study examines the impact of these SLNs on rotenone (RT) caused Parkinson's disease (PD) in both rat and zebrafish models. The process of loading SC into SLNs was achieved through the solvent evaporation-emulsification method. The SC-encapsulated solid lipid nanoparticles (SCSLNs) were subjected to physicochemical evaluation, and their properties were verified. For 28 days, the rats received subcutaneous injections of RT at a dosage of 2 mg × kg^{-1} body weight. Additionally, the rats in the experimental group received SCSLNs from the 14th to the 28th days of the trial. Interestingly, the locomotor activity, grip strength, and exploratory behaviour of the rats with SCSLNs significantly improved. Furthermore, it was observed that the quantities of acetylcholinesterase (AchE) inside the brain tissue had increased, and oxidative biomarkers had decreased. In addition, there was a discernible decrease in Lewy body development and cellular damage compared to the positive control group. Zebrafish were dosed with SCSLNs simultaneously as they were subjected to a 5 µg × L^{-1} RT concentration for 28 days during the experiment. AchE levels in the fish brain increased, resulting in improved locomotor activity in the SCSLN group of zebrafish. The findings of this investigation imply that using SCSLNs may reduce Parkinson's disease symptoms via enhanced delivery of SC into the brain.

Keywords Parkinson's disease, Targeted delivery, SLNs, S-carboxymethyl-L-cystine, Zebrafish

Abbreviations

AchE	Acetylcholinesterase
ANOVA	Analysis of Variance
BBB	Blood–Brain Barrier
BSA	Bovine Serum Albumin

[1]Department of Pharmacology, Faculty of Pharmacy, M S Ramaiah University of Applied Sciences, Mathikere, Bengaluru 560054, Karnataka, India. [2]Department of Pharmaceutical Chemistry, Faculty of Pharmacy, M S Ramaiah University of Applied Sciences, Mathikere, Bengaluru 560054, Karnataka, India. [3]Chromed Biosciences Pvt Ltd, Tumkur 572168, Karnataka, India. [4]Department of Pharmaceutical Chemistry & Analysis, School of Pharmaceutical Sciences, Vels Institute of Science, Technology & Advanced Studies, Pallavaram, Chennai 600117, Tamil Nadu, India. [5]Department of Pharmacology, College of Pharmacy, King Khalid University, Abha 61421, Saudi Arabia. [6]Department of Biotechnology, Kalasalingam Academy of Research and Education, Krishnanakoil 626126, Tamil Nadu, India. ✉email: selvapharmabio@gmail.com; superdamu@gmail.com; pvpram@gmail.com

COMT	Catechol–O–methyltransferase
DA	Dopamine
DJ	1–Daisuke–Junko–1 (PARK7)
DTNB	5,5′–Dithiobis–(2–nitrobenzoic acid)
EE	Encapsulation Efficiency
FTIR	Fourier–Transform Infrared Spectroscopy
GSH	Glutathione
H&E	Hematoxylin and Eosin
IAEC	Institutional Animal Ethics Committee
LB	Lewy Bodies
LPO	Lipid Peroxidation
MDA	Malondialdehyde
MD	Molecular Dynamics
MM	GBSA–Molecular Mechanics Generalized Born Surface Area
MMP3	Matrix Metalloproteinase–3
NAC	N–acetylcysteine
NBT	Nitroblue Tetrazolium
OECD	Organisation for Economic Co–operation and Development
OPLS	4–Optimized Potentials for Liquid Simulations 4
PDB	Protein Data Bank
PD	Parkinson's Disease
PDI	Polydispersity Index
PL	Protein–Ligand
RT	Rotenone
RMSD	Root Mean Square Deviation
RMSF	Root Mean Square Fluctuation
ROS	Reactive Oxygen Species
SC	S–Carboxymethyl–L–Cystine
SCSLNs	S–Carboxymethyl–L–Cystine–Loaded Solid Lipid Nanoparticles
SD	Standard Deviation
SEM	Standard Error Mean / Scanning Electron Microscopy (based on context)
SLNs	Solid Lipid Nanoparticles
SOD	Superoxide Dismutase
TEM	Transmission Electron Microscopy
UV	Ultraviolet

Parkinson's disease (PD) is a progressive neurodegenerative ailment that affects around 8.5 million individuals worldwide, as reported by the World Health Organization in 2019. It ranks as the second most prevalent neurodegenerative condition, surpassed only by Alzheimer's disease[1]. It is projected that the incidence of PD will increase two-fold to reach 12.9 million cases by the year 2040, thereby establishing it as an escalating concern within the healthcare domain[2]. The cardinal manifestations of PD commonly include motor impairments such as tremors, bradykinesia, rigidity, and postural instability. Additional clinical features encompass non-motor symptoms such as autonomic dysfunction, cognitive impairments, sleep disturbances, and sensory abnormalities, including anosmia and pain. Furthermore, secondary motor symptoms encompass hypomimia, dysarthria, dysphagia, shuffling gait, festination, freezing, and dystonia[3]. The initial rapid degeneration of dopamine distinguishes PD (DA) neurons in the midbrain, followed by a gradual formation of Lewy bodies (LB) in the brain. The invasion of the neocortex by LB is associated with observable indications of dementia. Individuals who have a higher age, over 70 years, tend to develop dementia at an earlier stage. Further, their brains exhibit a significantly more significant presence of LB, which is characterized by the accumulation of α-synuclein[4].

Several animal models are currently being utilized to simulate PD to investigate its underlying mechanisms and discover novel therapeutic strategies for its amelioration and treatment. Various moieties have been examined for their potential anti-PD action in rat models caused by radiation therapy. *Danio rerio*, also known as Zebrafish, has emerged as a promising and increasingly utilized animal model for studying several neurodegenerative disorders. The utilization of *Danio rerio*as a model organism for studying neurologic disorders is attributed to several key advantages. These advantages include its physiological similarity to humans, rapid replication cycle, cost-effectiveness in breeding, and suitability for conducting drug screening studies[5]. Numerous studies have extensively analyzed and documented the implications of its application in PD modeling[6–8].

S-carboxymethyl-L-cystine (SC), a neuroactive drug gaining popularity for its potential clinical application in treating neurological illnesses, is frequently used for various pathologies. S-carboxymethyl-L-cystine (SC) is a sulfur-containing amino acid derivative, specifically the carboxymethyl derivative of cysteine. This compound has been recognized and accessible for about eight decades. Throughout its history, this particular entity has been utilized for many purposes. However, within the realm of respiratory medicine, it has established a distinct and valuable role. Initial research suggested that this chemical followed a straightforward and predictable metabolic pathway. However, subsequent examinations suggested that it exhibited more intricate interactions with intermediary metabolic pathways, which aligns with what one would anticipate for an amino acid derivative[9].

SC is an amino acid that contains sulfur and is not naturally occurring. It can be seen as a thioether derivative of cysteine. The absence of a free thiol group suggests that the antioxidant mode of action differs from that of cysteine or other readily accessible mucolytic cysteine derivatives, such as N-acetylcysteine (NAC). NAC

possesses a single unbound sulfhydryl (thiol) group capable of interacting with the disulphide bonds in mucus glycoproteins. This interaction leads to an elevation in mucus viscosity. In contrast, SC does not directly engage with the disulphide bonds of glycoproteins[10]. The proposition posits that NAC may confer cellular protection against oxidative damage by its direct scavenging activity, facilitated by its free thiol group, leading to the formation of NAC disulphide. However, it is essential to note that this assertion lacks robust scientific substantiation[11]. Cysteine serves as the amino acid substrate that restricts the rate of intracellular synthesis of glutathione. Research has demonstrated that when present in low concentrations, thiol amino acids such as cysteine and NAC primarily function as antioxidants by augmenting glutathione levels rather than directly scavenging reactive oxygen species. In contrast, sulfur-containing amino acids such as methionine possess a thioether link susceptible to oxidation by reactive oxygen species (ROS), resulting in sulfoxide formation. The ability of the SC mechanism to act as a scavenger of free radicals was investigated in both a cellular system devoid of external influences and in activated human polymorphonuclear neutrophils. The results suggest that SC, like methionine, possesses potent and selective scavenging capabilities against OH and HOCl, which are highly detrimental free radicals responsible for inducing substantial harm to tissues[12].

Consequently, in the last couple of decades, several research efforts have been devoted to formulating nanosized lipid-based pharmaceutical dosage forms to bypass the obstacle represented by the blood-brain barrier (BBB) and reach the central nervous system (CNS). Nanoparticles are solid colloidal particles within the size range of 10 to 1000 nm (1.0 μM). These particles carry active principles, such as drugs or physiologically active materials, which can be dissolved, entrapped, adsorbed, or connected to the nanoparticles[13]. Solid lipid nanoparticles (SLNs) are colloidal dispersions in an aqueous medium characterized by a matrix composed of biodegradable lipids[14]. SLNs provide the capacity to integrate the benefits while circumventing the limitations of various colloidal carriers within their category. These advantages include enhanced physical stability, safeguarding susceptible pharmaceuticals against degradation, regulated release mechanisms, and exceptional tolerability[15,16]. In light of the aforementioned research information, the present study involved the development of SLNs utilizing SC to investigate its potential therapeutic effects in mitigating the symptoms associated with Parkinson's disease.

Experimental section

Methods

All experiments were conducted according to the guidelines of the National Institutes of Health Guide for the Care and Use of Laboratory Animals and were approved by the Scientific Investigation Board of the institutional animal ethical committee of MS Ramaiah University of Applied Sciences as taken to minimize suffering and the number of animals used in the experiments.

Experimental animals

The Wistar rats and Zebra fish (*Danio rerio*) used in this study were obtained from the Department of Pharmacology, Faculty of Pharmacy, MS Ramaiah University of Applied Sciences, Bengaluru, India. Form B (per 8(a)* for Submission of Research Protocol Application for Permission for Animal Experiments was approved by the Institutional Animal Ethics Committee (IAEC) and submitted to CPCSEA, New Delhi, before the commencement of the study. Approved under approval number XXVII/MSRFPH/COL/PG-05/13.02.2023 by the Institutional Animal Ethics Committee of the Department of Pharmacology, Faculty of Pharmacy, M.S. Ramaiah University of Applied Sciences, the study protocol was approved during a meeting on February 13th, 2023.

The rats had an average 180–220 g weight and were between 6 and 8 months old. Both male and female rats were included in this study. The animals were housed in polyacrylic enclosures furnished with comfortable bedding materials. The experimental conditions were maintained as per standard animal husbandry protocols, including a 12-hour light-dark cycle and *ad libitum* access to food and water. Also, the study employed 48 wild-type Zebrafish (*Danio rerio*), encompassing individuals of both sexes, with an age range between three and four months. The Zebrafish had an average initial body weight of 0.9 ± 0.1 g. The Zebrafish were acquired from the Department of Pharmacology, Faculty of Pharmacy, MS Ramaiah University of Applied Sciences (MSRUAS), Bengaluru, India. The Zebrafish were placed in a 5 L acrylic fish aquarium, and a minimum of 10 days was allowed to acclimate before the commencement of the experiment. The aquariums, namely the housing and experimental tanks, were filled with filtered facility water. The water temperature was maintained at a constant level of 26 ± 2 °C. White fluorescence lamps were utilized to provide illumination, following a cycle of 14 h of light and 10 h of darkness. The organisms in the tanks were fed three times daily.

Drugs and chemicals

SC and RT were procured from BLD Pharm and Merck, Bengaluru, India. Reagents and solutions used for the formulation of SLNs and the rest of the study were of analytical grade and freshly prepared before use.

Target identification

The collection of targets for the active elements of Swivel-Derived Exhaled Breath Condensate (SEBC) and PD was facilitated through the utilization of the following platforms: Genecards[17], OMIM Swiss target prediction[18], Gprofiler[19], ShinyGO[20], and Venn diagram[21]. Venn diagrams are visual depictions that illustrate sets using intersecting circles. Within the domain of PD, Venn diagrams serve as a valuable tool to graphically analyze and juxtapose distinct groups of components or variables that may exhibit associations with the ailment above. The circles denoting each category of PD would intersect, illustrating the shared risk factors between the two types and the distinct risk factors specific to each type.

Network Pharmacology

The protein interaction network (hsa05012) of PD in *Homo sapiens* was selected for the identification of influential proteins. The Kyoto Encyclopedia of Genes and Genomes database (https://www.genome.jp/pathway/hsa05012) was used to conduct a graph theoretical analysis[22,23].

Selection and Preparation of protein and active compound retrieval

The protein targets that are related to and have a significant relation to PD were identified. These crystal structures of proteins MMP3 (matrix metalloproteinase-3) (1HY7), Human endothelial nitric oxide synthase (PDBID: 1M9M) MAO B (Monoamine Oxidase B) (PDBID: 2BYB), COMT (Catechol-O-methyltransferase) (PDB ID: 6I3D), NCS 1 (Neuronal calcium sensor-1) (PDB ID: 6QI4), Protein deglycase DJ-1 (PDBID: 6AFI) in complex with the standard drug were identified from Research Collaboratory for Structural Bioinformatics Protein Data Bank (PDB: http://www.rcsb.org/pdb). The proteins were prepared using Charmm-GUI (https://www.charmm-gui.org/) by adding missing residues and removing co-crystallized ligands and water molecules. The structure of S-carboxymethyl-L-cystine was retrieved from the public database PubChem (https://pubchem.ncbi.nlm.nih.gov/).

Docking procedure

The grid was generated using the Maestro viewer v13.9 of Schrodinger (https://www.schrodinger.com/products/maestro) software. The prepared co-crystallized protein was pre-processed and optimized in Maestro. Then, a grid was generated by taking the standard ligand bound to the co-crystallized protein as the center, and the grid coordinates were noted. The crystallized structure of the proteins without the standard ligands was taken. Using Autodock 4.2 (https://autodocksuite.scripps.edu/), the reported coordinates were added to generate the grid box, and the S-carboxymethyl-L-cystine ligand was docked to the protein. Furthermore, the amino acids that interacted with the ligand were noted using the 2D image of the complex. The docking scores were compared with the standard ligands. Protein-ligand interactions were visualized using BIOVIA Discovery Studio 2021 (https://discover.3ds.com/).

Molecular dynamics simulation

Molecular dynamics (MD) simulation analysis was conducted to investigate the stability and fluctuation of a protein-ligand complex, using the Linux operating system, employing the Desmond module (https://www.schrodinger.com/platform/products/desmond/) and the Maestro simulation environment developed by Schrodinger for a time period of 100 ns. The TIP3 water model, featuring a cubic box shape boundary constraint, addressed the intricate protein-ligand interaction. The system was rendered inert by introducing Na^+ and Cl^- salt concentrations at 0.15 M. MD simulation was conducted using the NPT ensemble, which maintains constant pressure (1.01325 bar) and temperature (300 K). The simulation employed recording intervals of 50 picoseconds (ps) and utilized the 1.2 OPLS-4 force field for energy calculations. The stability of the ligand-protein complexes was assessed by employing various metrics, including root-mean-square deviation (RMSD), root-mean-square fluctuation (RMSF) and analysis of protein-ligand interactions derived from the simulated trajectories.

Preparation of SCSLNs

S-carboxymethyl-L-cystine-loaded solid lipid nanoparticles (SCSLNs) were prepared using the solvent evaporation-emulsification approach, employing a high-speed homogenizer and an ultra-sonicator. Stearic acid (1 g) and SC (2 mg) were dissolved separately in chloroform (5 mL) and methanol (5 mL), respectively, and afterward mixed. The organic solution obtained was subjected to homogenization in a 50 mL aqueous solution containing a surfactant (1% tween-80) and co-surfactant (0.5% sodium deoxycholate). This homogenization process was carried out using the Ultra Turrax T25 homogenizer (IKA, Bengaluru, India) at 15,000 rpm for 30 min, forming SLNs. The SCSLNs formulation underwent sonication using a probe sonicator with a voltage efficiency of 35% for 10 min. Subsequently, it was subjected to continuous stirring overnight using a magnetic stirrer to ensure the total elimination of organic solvents.

Encapsulation efficiency (EE) & loading capacity (LC)

The SC into SLNs EE and LC were determined as per the previously reported method with slight modifications[24]. Concisely, the concentration of the supernatant (not included within capsules) following centrifugation of the synthesized nanoparticles was determined by assessing the absorbance at 245 nm using a UV-visible spectrophotometer after subjecting the samples to centrifugation for 30 min at 4 °C and 15,000 rpm. The SC content was determined by extrapolating the absorbance values using a standardized calibration plot. The estimation of SC EE was conducted utilizing the subsequent equations:

$$\% \text{ EE} = [(\text{Total amount of SC added - free SC})/\text{Total amount of SC added}] \times 100.$$

$$\% \text{ LC} = [(\text{SC})\text{added} - (\text{SC})\text{measured} / \text{SLNs weight}] \times 100.$$

Drug release study

The previously studied dialysis bag diffusion method[43] was followed to study pH-dependent SC release from SCSLNs. The viscous solutions of SCSLNs were poured into Petri plates (7 cm in diameter) and placed in a freezer at −20 °C for 12 h, followed by lyophilization for 24 h to achieve complete drying. 50 mg lyophilized SCSLNs in 5mL deionized water was added to the dialysis bag (3500 Da molecular weight cut off) and tightly sealed. The setup was immersed in 100 mL of 0.01 M acetate buffers with varied pH 3.2, 5.4 and 0.01 M phosphate buffer at pH 7.2 systems, stirred at 100 rpm at 37 °C ± 2 °C. The experimental container was carefully wrapped with aluminum foil to prevent buffer solution loss. At the pre-fixed time point, the released drug samples were extracted (2 mL of released medium was collected and swapped with an equivalent volume of new, diluted buffer

solution). The mixture was centrifuged at 10,000 ×g at 25 °C to separate the oil layer from the buffer system and estimate released SC via UV-visible spectroscopy. The tests were carried out in triplicate. The formula for calculating cumulative drug release (% DRC) was as follows:

$\%DRC = (A_0 - A_1) \times 100/A_0$.

where, A_0 = absorbance of the control; A_1 = absorbance of SC.

Stability studies

In vitro stability studies of freshly prepared SCSLNs were carried out using various physiological mediums (10% NaCl, 0.5% BSA), acetate buffer solution pH 3, 5, and phosphate buffer solutions pH 6, 7.4, and 9. Concisely, 0.5 mL of SCSLN suspension was mixed with 0.5 mL of each physiological medium and phosphate buffer solution, and the maximum absorbance was measured using a UV-visible spectrophotometer after 72 h.

Fourier-transform infrared spectroscopy (FTIR)

The FTIR spectra of SC and the physical mixtures of the drugs with each polymer, namely sodium deoxycholate, stearic acid, and Tween 80 (at a 1:1 w/w ratio), were obtained using a Thermo Scientific™ Nicolet™ iS-50 Fourier-transform infrared spectrometer sample holder. The FTIR spectroscopy was conducted in the wavelength range of 4000 to 500 cm^{-1} with a resolution of 4 cm^{-1}, and a total of 25 scans were combined. The absorbance and intensity of the characteristic peaks for the sample compound (SC) and its corresponding polymer were detected and recorded in the spectral regions of interest.

Particle size and zeta potential analysis

The SCSLNs mean size (z average) was measured by the photon-correlation spectroscopy (PCS) method using Shimadzu SALD-2300 instruments. All measurements were performed at 25 °C at a detection angle of 90°. The zeta potential was measured using the same instrument. Zeta potential is the charge exhibited by a solid lipid nanoparticle surface. It can be used to optimize the formulations[25].

Powder X-ray diffraction analysis

The physical attributes of SLNs were assessed utilizing the BRUKER D8 Advance ECO XRD equipment equipped with the SSD160 1D Detector. A fully desiccated, slender layer of the refined SLNs containing the active compound SC was positioned, and the sensor functioned at a voltage of 20-kilo electron volts (keV) and a current of 30 milliamperes (mA) using copper K-alpha 1 radiation (1 = 1.54060) in a 2θ configuration[26].

Scanning electron microscopy (SEM)

The surface morphological properties of freshly made solid lipid nanoparticles (SLNs) loaded with SC material were obtained using a Carl Zeiss EVO SEM instrument. The experimental procedure involved placing a representative sample of SCSLNs onto a copper grid with a 200-mesh size. Subsequently, the sample was subjected to observation using a Scanning Electron Microscope (SEM) to determine the form and size of the particles[27].

Transmission electron microscope (TEM)

The evaluation of the size and shape of SLNs was conducted using a TEM with a JEOL model 2100, operating at an acceleration voltage of 200 kV. SCSLNs were re-dispersed using 1 mL of deionized water to achieve this objective. A small quantity of dispersed SCSLNs sample was applied onto a carbon-coated copper grid and dried in ambient air at 60 °C for 5 min[27].

In vivo **pharmacological evaluation**.

Experimental animals

The study is reported by ARRIVE guidelines (https://arriveguidelines.org). The breeding facility at the institution supplied male Wistar rats weighing 150–160 g and 9 weeks old. The rats were acclimated for 7 days at 25 ± 2 °C and 55 ± 1% relative humidity in a clean environment with a 12-hour light/dark cycle. They were given a typical pellet feed and endless access to water. The protocols of the Committee for the Control and Supervision of studies on Animals (CCSEA), located in New Delhi, India, were followed in all studies. Authentication number IAEC Ref No.: XXVII/MSRFPH/COL/PG-05 was issued after the study protocol was approved by the Institutional Animal Ethics Committee of the Department of Pharmacology, Faculty of Pharmacy, M.S. Ramaiah University of Applied Sciences, at a meeting on 13.02.2023 for the use of Wistar rats and zebra fish.

Acute toxicity studies of SLNs in Wistar rats

Acute oral toxicity studies were followed according to OECD 423 guidelines[28]. Since we were using SLNs for targeted drug delivery, of SCSLNs formulation and bulky nature, a maximum dose of 300 mg × kg^{-1} was administered.

Acute toxicity studies in zebrafish

Zebrafish toxicity was performed based on OECD guidelines 203[29]. A group comprising 7 fish were treated with SCSLNs. All fishes were fasted 24 h before the experiment. SCSLNs was added to the tank at a maximum concentration of 2500 μg × L^{-1} and the experiment was carried out for 96 h.

Experimental design

For Wistar rats, RT (dissolved in sunflower oil to get the final suspension containing 1.5 mg rotenone/mL) was injected subcutaneously into rats for 28 consecutive days. Forty-two rats were randomly divided into seven groups, each containing six. Animals were evaluated for behavioral changes and biochemical parameters. Group

1: Rats received saline (1 mL× kg^{-1} body weight (b.w) per day orally) for 28 days to serve as the control. Group 2 (Positive control): Rats were treated with RT (2 mg× kg^{-1} b.w per day for 28 days in subcutaneously). Group 3 (standard): Rats were treated with RT (2 mg× kg^{-1} b.w per day for 28 days subcutaneously) + Levodopa (5 mg × kg^{-1} b.w in per oral (p.o)) + Carbidopa (5 mg × kg^{-1} b.w in p.o). Group 4 (low dose): Rats were treated with RT (2 mg× kg^{-1} b.w per day for 28 days in subcutaneously) + SCSLNs (15 mg × kg^{-1} b.w). Group 5 (medium dose): Rats were treated with RT (2 mg× kg^{-1} b.w per day for 28 days in Subcutaneous) + SCSLNs (30 mg × kg^{-1} b.w in p.o). Group 6 (high dose): Rats were treated with RT (2 mg × kg^{-1} b.w per day for 28 days in Subcutaneous) + SCSLNs (60 mg × kg^{-1} b.w in p.o). Group 7 (unformulated): Rats were treated with RT (2 mg × kg^{-1} b.w per day for 28 days in Subcutaneous) + S-Carboxymethyl-L-Cystine (100 mg × kg^{-1} b.w per day for 28 days in p.o).

Beam walk

This task necessitates an animal to traverse a small wooden beam, thereby evaluating its motor coordination proficiency. The beam consisted of two platforms (8 cm in diameter) joined by a wooden beam (10 mm in thickness, 2.0 cm in width, and 120 cm in length). The beam was raised to a height of 50 cm above the ground. A container with sawdust was positioned beneath the beam, functioning as a safeguard for a descending rodent. Before starting the training session, a rat was allowed five minutes to become familiar with the raised beam. The rat was placed onto the platform at one end to begin the training. Every experimental iteration's time to cross the beam was timed and recorded[30].

Wire test

Rats were used to measure their physical strength using the wire grasp test. The rats hung with their forepaws resting on a 60-centimeter-long, 7-millimeter-diameter horizontal steel wire. The animals sat up straight when their front paws contacted the wire. A stopwatch measured the length of time an animal descended from the wire. Rats were chosen at random for the experiment, and each rat received a single trial[31].

Open-field test

An instrument designed expressly to assess several behavioral responses, including locomotor activity and exploratory behavior, is the open-field test. An experimental square enclosure of 76 centimetres by 76 centimetres was used in the open-field test. The enclosure's walls, which were made of an opaque material, were 42 centimeters high. The flooring is partitioned into 25 congruent squares. To observe the behavior of animals, individuals were removed from their respective home cages and sequentially placed in the center square of an open field. The measurement of distance covered and average velocity calculation were recorded for 5 min[32].

Processing of the brains

After assessment of the motor performance, rats were euthanized by injection of ketamine and xylazine (80 mg/kg: 12 mg/kg, i.p.). Brains were quickly dissected and washed with ice-cold saline. The whole brain was homogenized in 5 M phosphate buffer. The homogenate was further processed for oxidative parameters and AchE estimation.

Malondialdehyde (MDA)

A mixture of 1 mL of TBA: TCA: HCl was introduced into a solution containing 500 µL of brain homogenate, which was produced using potassium chloride (0.15 M) at a concentration of 10% w/v. Subsequently, the mixture was boiled for 15 min, followed by a cooling process and subsequent centrifugation at 10,000 revolutions per minute for 5 min. The solution containing the supernatant was separated, and the absorbance was measured at a wavelength of 532 nm relative to a reagent blank. The concentration of malondialdehyde (MDA) was determined by measuring the reaction of thiobarbituric acid with MDA and quantified as nmol/100 mg of tissue. The calculation used a molar extinction coefficient of 1.56×10^5 moles × cm^{-1}[33].

Catalase

A total of 1.9 mL of phosphate buffer solution with a pH of 7 was combined with 100 µL of brain homogenate, which was made using a 0.15 molar potassium chloride buffer and had a concentration of 10% weight/volume. After introducing 1 mL of a 10 mM H_2O_2 solution, absorbance was measured at a wavelength of 240 nm at time zero. The observed decline in absorbance after introducing 1 mL of H_2O_2 was again recorded after 1 min. Catalase activity was determined through the utilization of the molar extinction coefficient of $H_2O_2$and subsequently quantified in units per milligram of wet tissue[34].

Glutathione (GSH)

A brain homogenate with a sucrose concentration of 10% w/v was made in a phosphate buffer solution at a pH of 7.4. This homogenate was utilized to determine the levels of glutathione (GSH) using a method that had been previously described[35]. A volume of 200 µL of Ellman's reagent was introduced into the reaction mixture, and after 5 min incubation, the absorbance was measured at a wavelength of 412 nm. GSH was quantified and thereafter reported as nmol per 100 mg of tissue.

Superoxide dismutase (SOD)

A total of 50 µL of a homogenate with a concentration of 10% weight/volume was combined with 0.5 mL of a sodium carbonate solution with a concentration of 100 mM, along with 200 µL of NBT (24 millimolar in methanol) and 100 mL of EDTA with a concentration of 1 mM. Following the addition of 200 µL of hydroxylamine hydrochloride with a concentration of 1 mM, a reading at 560 nm was taken at time zero. The mixture underwent

incubation for 5 min, after which the reduction of NBT was assessed after an additional 5-min period at a wavelength of 560 nm. The enzymatic unit of superoxide dismutase (SOD) refers to the quantity of the enzyme found in 100 µL of a 10%w/v tissue homogenate that is necessary to impede the reduction of 24 mM NBT by 50%. This unit is typically given as U/mg of wet tissue[36].

AChE enzyme

A 0.4 mL portion of the homogenate is introduced into a cuvette containing 2.6 mL phosphate buffer solution (0.1 M, pH 8) and 100 µL of DTNB. The cuvette's contents are well mixed, and the absorbance is subsequently measured at a wavelength of 412 nm using a spectrophotometer. A volume of 20 µL of the substrate, namely acetylthiocholine, is introduced into the experimental setup, and the resulting alteration in absorbance is measured. The determination of the change in absorbance per minute is therefore established[37].

Histopathology

The entire brain tissues were perfused and preserved in a 10% neutral buffered formalin solution for 72 h. The samples underwent a series of procedures for preparation, including dehydration in alcohol, clarifying in xylene, synthetic wax infiltration, and blocking out into Paraplast® tissue embedding media. Sagittal brain slices of three to five micrometers were obtained using a rotatory microtome. The slices underwent staining with Hematoxylin and Eosin (H&E), a commonly used staining procedure for general investigation. Additionally, Nissl staining was performed using toluidine blue to visualize both intact and injured neurons.

Pharmacological studies using the zebrafish model

For zebrafish, RT was dissolved in DMSO and made up with water. 40 fishes were randomly divided into 5 groups, each containing 8 fishes. The system was replaced every 2 days. Animals were evaluated for behavioral changes and biochemical parameters after the last dose. 5 $\mu g \times L^{-1}$ of RT for 28 days was effective in inducing PD from our initial validation study, and the same dose was used to induce PD in the main objective. Animals were evaluated for behavioral changes and biochemical parameters after the last dose. Group 1 (Negative control): Fishes received vehicle. Group 2 (Positive control): Fishes were treated with RT (5 $\mu g \times L^{-1}$ for 28 days). Group 3 (high): Fishes were treated with RT (5 $\mu g \times L^{-1}$ for 28 days) + SCSLNs (500 $\mu g \times L^{-1}$). Group 4 (low): Fishes were treated with RT (5 $\mu g \times L^{-1}$ for 28 days) + SCSLNs (250 $\mu g \times L^{-1}$). Group 5 (unformulated): Fishes were treated with RT (5 $\mu g \times L^{-1}$ for 28 days) + SC (1000 $\mu g \times L^{-1}$).

Swimming behavior recording

The evaluation of swimming behavior was conducted utilizing the ID player program (https://www.idtracker.es/). A 5-litre tank with a white coloration was utilized as the assay tank. The tank was positioned on a platform that provided stability and filled with plant water after filtration. The experimental environment was enclosed by cardboard boxes, creating a physical barrier. Additionally, the experiment was conducted in a secluded room to mitigate the influence of external visual and aural distractions. The provision of illumination was facilitated with the utilization of LED lighting. A camera was put on top of the tank to catch the top view and recorded for 5 min. The videos were stored in the .mp4 file format.

Swimming behavior analysis

The swimming behavior was defined as locomotor activity. The locomotor activity was evaluated in terms of total distance travelled, which was analyzed using the ID player (https://www.idtracker.es/)[38].

Acetylcholine esterase Estimation in zebrafish

The zebrafish were decapitated, eyes were removed, and an entire head of the animal was homogenate and placed in ice-cold saline. 4 fish were sacrificed from one group owing to the small size of the zebrafish to get sufficient homogenate. The tissues are carefully measured and then subjected to homogenization in a 0.1 M Phosphate buffer solution with a pH of 8. A 0.4 mL portion of the homogenate is introduced into a cuvette containing 2.6 mL of phosphate buffer solution with a concentration of 0.1 M and a pH value of 8. Additionally, 100 µl of DTNB is included in the cuvette. The cuvette's contents are thoroughly mixed, and the spectrophotometer is used to measure the absorbance at a wavelength of 412 nm. A volume of 20 µL of the substrate, namely acetylthiocholine, is introduced into the experimental setup, and the resulting alteration in absorbance is measured. The determination of the change in absorbance per minute is therefore conducted.

Statistical analysis

Data are expressed as Mean ± Standard Error Mean (SEM). The gathered values were subjected to One-way Analysis of Variance (ANOVA) for comparison, followed by the Tukey-Kramer test for conducting multiple comparisons. In statistical analysis, the convention of denoting significance levels is commonly employed. A significance level of $^{*}p < 0.05$ is typically interpreted as indicating mild statistical significance. Similarly, $^{**}p < 0.01$ generally represents moderate statistical significance, while $^{***}p < 0.001$ indicates high statistical significance. Lastly, the notation $^{****}p < 0.0001$ designates extremely significant findings[39].

Results

Target identification

The SCSLNs for the treatment of PD were investigated by using targets of SC and targets of PD through Venn diagrams. The following platforms, Genecards, OMIM Swiss target prediction, and Venn diagram, were used to generate data sets of targets Supplementary Fig. 1(a). Venn diagrams are graphical representations of sets using overlapping circles. In the context of PD, Venn diagrams can be used to visually compare and contrast different

sets of factors or variables that may be related to the disease. The circles representing each type of PD would overlap to show the common risk factors shared by both types and the unique risk factors for each type. Venn diagrams can also be used to visualize the relationship between different biomarkers or genetic mutations that may be associated with PD. The circles representing each biomarker or mutation would overlap to show the commonalities and differences between them. This can help identifying potential 28 targets for treatment or further research. Identified common 28 targets are introduced into the graphical network for further evaluation to pick significant targets for PD treatment.

PARK7/DJ-1 MMP2 GRM2 GRIK2 ENPEP SLC1A3 PTPN1 GRIK5 SLC1A1 GRM4 CACNA2D1 GRM6 GRM1 SLC7A11 GLO1 GRM8 FDPS GRIA2 NOS2 GRM3 GRIK3 SLC1A2 GRIK1 GRM5 PYGM GRIA1 ADORA3 GRM7 GRIA4.

Network pharmacology

The pathway was renewed as a graph using hsa05012 by proteins (nodes) and interactions (edges) and it was represented in Supplementary Fig. 1(b) and Table 1. The network carries 114 nodes and 147 edges; the significance of proteins was identified by calculating the value of parameters. Based on the average measure of each parameter leads to obtaining high-significance proteins such as PARK7/DJ-1PRKN CYCS HSPA5 DAXX LRRK2 RPS27A UBE2L3 RPS27A SNCAIP UCHL1 RPS27A TH CASP9 ADCY5 PRKACA DDIT3 SNCAPSMA8 CALML6 KLC3 PRKN BAX PARK7/DJ-1 L1 TP53 MAP3K5 NFE2L2 SNCA MCU and C22381. Among the best 114 nodes, the observed results of PARK7/DJ-1 was having Centrality score of 10,566 as Stress, Centrality score of 8.495145631 as Radiality, Centrality score of −0.654033901 as Eigenvector, Centrality score of 0.005102041 as Closeness, a Centrality score of 0.125 as Eccentricity, a Centrality score of 4541.575942 as Betweenness and a Centrality score of 18 as Degree from the network. The target PARK7/DJ-1 were identified as a drug target for the PD treatment based on significant measures with its threshold values mentioned in Table 1 and Supplementary Fig. 1(b). PARK7/DJ-1 has more attention because of its interaction with PD proteins which

Label	Degree	Betweenness	Closeness	Eccentricity	Eigenvector	Radiality	Stress
PARK7/DJ-1	18	4541.58	0.005	0.125	−0.6540	8.4951	10,566
PRKN	6	979.94	0.003	0.083	−0.0049	7.2427	3028
CYCS	5	478.99	0.003	0.091	−0.0122	7.1360	928
HSPA5	4	903.85	0.003	0.083	−0.0025	7.1845	1632
DAXX	4	156.67	0.004	0.111	−0.2352	7.8835	242
LRRK2	3	429.97	0.004	0.111	−0.1543	7.9806	862
RPS27A	3	1269.50	0.004	0.111	−0.1556	8.2427	4040
UBE2L3	3	851.54	0.003	0.091	−0.0172	7.3883	3034
RPS27A	3	716.18	0.004	0.1	−0.0387	7.9320	2270
SNCAIP	3	232.51	0.003	0.077	−0.0014	6.7282	418
UCHL1	3	130.71	0.003	0.083	−0.0020	6.8738	424
RPS27A	3	96.02	0.003	0.083	−0.0022	6.8155	338
RPS27A	3	120.16	0.003	0.077	−0.0008	6.7087	244
TH	3	419.82	0.004	0.111	−0.1628	7.8738	1256
CASP9	3	179.30	0.003	0.083	−0.0047	6.5922	474
ADCY5	3	325.84	0.003	0.071	−0.0002	5.5728	862
PRKACA	3	508.35	0.002	0.083	−0.0036	6.5631	1616
DDIT3	3	143.49	0.002	0.067	−0.0001	5.8544	566
SNCA	3	888.04	0.003	0.091	−0.0097	7.6019	1586
PSMA8	3	358.71	0.003	0.077	−0.0011	6.5922	1346
CALML6	3	521.68	0.004	0.111	−0.1543	7.9903	1104
KLC3	3	610.39	0.004	0.111	−0.1552	8.0097	1778
PRKN	3	0.75	0.004	0.111	−0.2189	7.9806	2
BAX	3	685.85	0.004	0.1	−0.0373	7.5631	1468
BCL2L1	3	919.65	0.004	0.111	−0.1545	8.0583	1836
TP53	3	152	0.004	0.111	−0.1987	7.8641	240
MAP3K5	3	145.88	0.004	0.111111111	−0.19999	7.8544	424
NFE2L2	3	287.38	0.004	0.111111111	−0.15480	7.8350	644
SNCA	3	131.05	0.003	0.1	−0.07285	7.4175	470
MCU	3	230.64	0.004	0.111111111	−0.16316	7.9320	886
C22381	3	19.85	0.003	0.1	−0.02687	6.8447	50

Table 1. The results of network analysis with threshold parameter values. Average Value of Degree 3; Betweenness 105.7561; Closeness 0.005869; Eccentricity 0.162115; Eigen Vector 0.084862; Radiality 4.634191; Stress 146.1471; Total Number of Edges 147 and Node 114.

is the cause of the spreading disease. Based on the graph theoretical analysis report and the significance of PARK7/DJ-1, it was chosen to be a noteworthy target through network pharmacology.

Mechanism of PARK7/DJ-1

PD is linked to the accumulation of PARK7 (Parkinson's disease protein 7), also known as DJ-1 (Daisuke-Junko-1). PARK7 interacts with alpha-synuclein, a protein that is found in clumps (Lewy bodies) in the brains of people with Parkinson's disease. Pathologically, the disease is characterized by the presence of these aggregates. PARK7 may play a role in regulating how much and how toxic alpha-synuclein aggregates Fig. 1.

Molecular docking studies

The docking score of SC with different targets was compared with the standard ligands of the respective targets. Along with the docking score the amino acid interactions of the target with the ligand were considered. Out of the various selected targets human endothelial MMP3, nitric oxide synthase, and DJ-1 showed a good binding score with SC, shown in Table 2. Furthermore, to these targets, SC binds with three active key amino acids namely ASN 76, CYS 106, and HIS 126 shown in Supplementary Fig. 2.

Molecular dynamics

Based on molecular docking studies, three complex SC-MMP3, SC-nitric oxide synthase, and SC-DJ-1 were further analyzed by MD simulation. MD simulation was carried out by Desmond tool using OPLS-4 force field

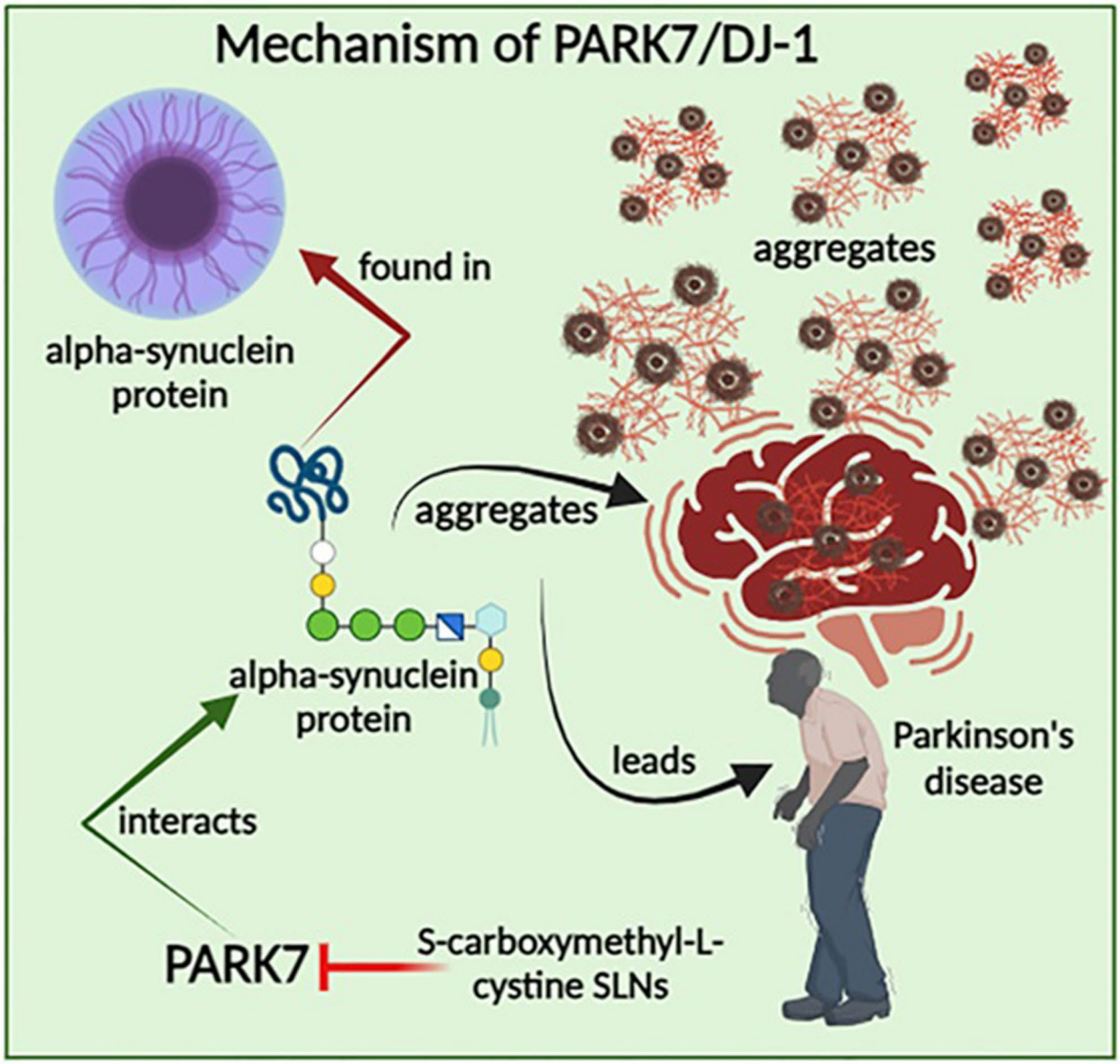

Fig. 1. Mechanism of PARK7/DJ-1.

Protein	PDB ID	Test		Standard	
		docking score (Kcal/mol)	Binding amino acids	docking score (Kcal/mol)	Binding amino acids
MMP3 (matrix metalloproteinase-3)	1HY7	−8.01	ASN662, LEU664, ALA665, VAL698, HIS701, TYR723	−8.55	LEU664, ALA665, HIS701, GLU704, LEU718, TYR723
Human endothelial nitric oxide synthase	1M9M	−7.44	CYS184, GLY186, PRO334, VAL336, GLY355, MET358	−8.26	PRO334, MET358, TYR375
MAO B (Monoamine Oxidase B)	2BYB	−4.51	SER59, TYR60, LYS296, MET436	−8.71	LEU171, CYS172, ILE199, GLN206, TYR326, PHE343, TYR398
Protein deglycase DJ-1	6AFI	−8.45	ARG48, ASN76, CYS106, HIS126	−8.98	GLU18, ASN76, GLY75, CYS106, ALA107, HIS126
COMT (Catechol-O-methyltransferase)	6I3D	−6.19	TRP88, MET90, ASP191, LYS194, ASP219, CYS223, GLU249	−8.58	ASP141, LYS144, ASP169, ASN170, GLU199
NCS 1 (Neuronal calcium sensor-1)	6QI4	−3.35	TYR52, THR92, LEU182	−5.01	TRP30, VAL68, LEU89

Table 2. Docking scores of active constituents with amino acids interaction.

S.No	Component	Role
1	**Formulation Process**	Modified solvent evaporation-emulsification process used for preparing SC-loaded SLNs
2	**Lipid Matrix Material**	Stearic acid, chosen for its high melting point, serves as the solid lipid core that forms the outer matrix of the nanoparticles
3	**Surfactant**	Tween 80, used to stabilize the nanoparticles in the aqueous medium
4	**Co-Surfactant**	Sodium deoxycholate, employed alongside Tween 80 to enhance nanoparticle stabilization and compatibility

Table 3. Formulation components of SCSLNs.

for 100 ns. The trajectory was analyzed to evaluate the selected complex's RMSD, RMSF, and protein-ligand interaction. Poor stability was observed for the SC-MMP3 complex and SC-nitric oxide synthase complex at the same time, the stability of SC-DJ-1 was found to be stable. Furthermore, the RMSD complex of SC-DJ-1 has a value within the range of 0.29 to 3.6 Å, protein-ligand, and PL contacts indicate the interaction of amino acids ARG 48 (interaction with Carboxylic OH) ASN 76 (interaction with Carboxylic OH, Carboxylic C = O & Primary NH_2). In addition, the results showed no variations in the RMSF of SC-DJ-1 throughout 100 ns. According to the molecular dynamic simulation findings, it was evident that SC-DJ-1 was engaging in significant contact with the 6AFI protein. As a result, SC-DJ-1 can potentially serve as an active lead moiety in treating PD (Supplementary Fig. 3).

SC-loaded SLNs (SCSLNs)

SC-loaded SLNs were prepared utilizing a modified solvent evaporation-emulsification process. In general, SLNs are a colloidal nanoparticulate system composed of a solid lipid as the matrix's outer layer, which surfactants stabilize in an aqueous environment. Stearic acid is used as the lipid matrix material during nanoparticle manufacturing since it has a greater melting point than the human body temperature. SC's biological action is mainly determined by its concentration, exposure time, and mode of delivery. Stearic acid, surfactant (tween 80), and co-surfactant (sodium deoxycholate) were selected based on compatibility and SCs physicochemical qualities, shown in Table 3.

Drug release

Figure 2(a) shows the cumulative release of SC from SCSLNs at 37 °C ± 2 °C in acetate buffers (pH 3.2 and 5.4) and phosphate buffers (pH 7.2). The release profile displays the cumulative percentage of medication released over time. The release of SC from SLNs was measured using validated UV-visible spectrophotometry. Figure 2(a) depicts the slow and steady release of the SC from SCSLNs. Within 60 min, SCSLNs emitted 8.22 ± 0.235% (pH 3.2), 8.803 ± 0.309% (pH 5.4), and 7.793 ± 0.49% (pH 7.2) of SC. After 5 h, approximately 15% (pH 3.2), 19% (pH 5.4), and 15% (pH 7.2) of SC were released from the SLNs, gradually increasing after the first 60 min. The pH variations had little effect on the SC release from the SCSLNs NPs. After 28 h, there was a consistent rise in the amount and rate of SC released from SCSLNs (70.107 ± 1.69%, 72.46 ± 2.04%, and 70.85 ± 1.634%, respectively) at pH 3.2, 5.4, and 7.2. Experiments showed that SC release from SCSLNs was more efficient at pH 5.4 than at neutral pH 7.2.

Stability studies

One of the major characteristics for SLNs in developing an efficient drug delivery system was stability in physiological fluids and various buffer solutions. Figure 2(b) shows the stability of freshly prepared SCSLNs in 10% NaCl (w/v), 0.5% BSA (w/v), acetate buffer solutions (pH 3.5 and pH 5), and phosphate buffer solutions (pH 6, 7.4, and 9). SCSLNs had a λmax of 230 nm in 10% NaCl (w/v), 0.5% BSA (w/v), and an acetate buffer solution at pH 3.5. SCSLNs exhibited 2–3 nm changes in λmax in acetate buffer pH 5, phosphate buffer pH 6, pH 7.4, and pH 9 medium. These findings reveal SCSLNs' outstanding stability under a variety of circumstances.

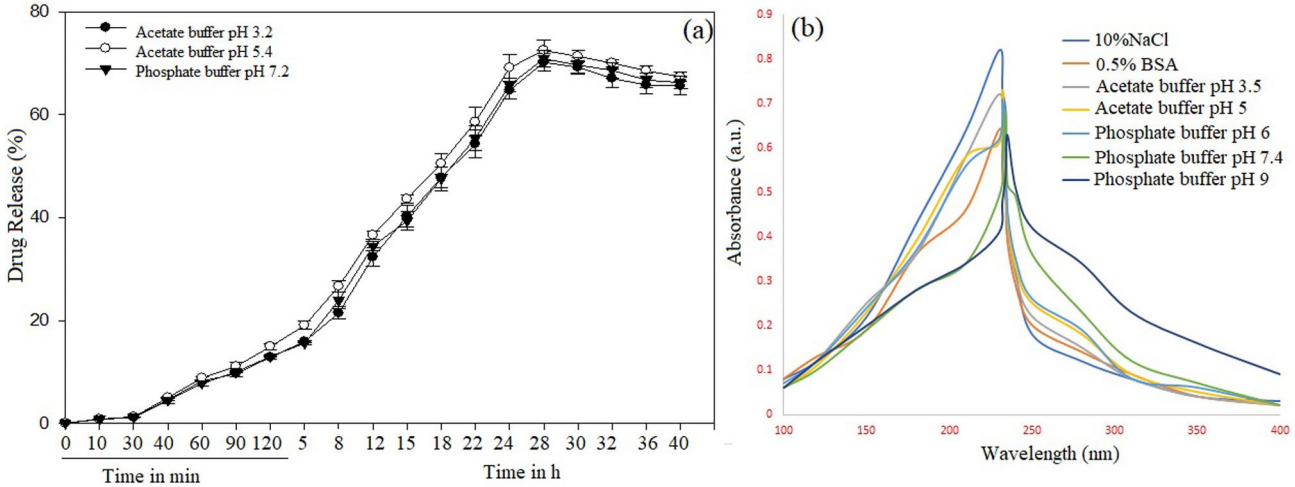

Fig. 2. In vitro SC (drug) release pattern of SCSLNs in acetate buffer (pH 3.2, 5.4) and phosphate buffer pH 7.2 at 37 °C as a function of time. Data are represented as mean ± standard deviation ($n = 3$) (**a**), The in vitro stability studies of SCSLNs in different physiological media and pH buffers.

Drug excipient compatibility and characterization of SCSLNs

As the procedure mentioned, freshly formulated SCSLNs and SC were scanned using an FTIR spectrophotometer. The peaks for SC were seen for OH grp at 3340 cm^{-1}, NH_2 grp at 3229 cm^{-1}, C = O group at 1634 cm^{-1}, C = C grp at 1556 cm^{-1} and C-S-C grp 1126 cm^{-1} and all of these peaks were retained when treated with the excipients. Therefore, the drugs and excipients are expected to be compatible with each other and free from any significant chemical interactions. The corresponding FT-IR spectrums are displayed in Fig. 3. Once the formulation was completed, the post-formulation FTIR was recorded. None of the SC peaks like the NH_2 group, C = C group and C-S-C group could be seen in the post-formulation FTIR, conforming the encapsulation of SC into sold lipid. The drug encapsulation efficacy was 91.1645%, and the loading capacity was 10.21%, which correlates with the post-FTIR studies. In particle size analysis, a prominent peak was obtained at 96.79 nm, with an average particle size of approximately 100 nm (Fig. 4(a)) and PDI of 0.504, validating the nanoparticle size and homogeneity of the formulation. The zeta potential of the SCSLNs was − 5.79 mv (Fig. 4(b)), indicating high stability. The XRD patterns exhibited sharp peaks with high intensity with slight changes in theta and d values, indicating that the final formulation has a crystalline structure (Fig. 5). The SEM images showed agglomeration, which may have resulted from lyophilization, but the TEM images indicate a clear and almost spherical structure of the SCSLNs. The corresponding SEM and TEM images of the SCSLNs were displayed in Figs. 6 (a), (b) and 6(c), (d), respectively.

Acute toxicity study

The acute toxicity study was conducted as per OECD guideline 423 using Wistar rats. There were no significant effects on the central and autonomic nervous systems or on sensory, gastrointestinal, cutaneous or respiratory functions during the 14-day observation period following the oral administration of SCSLNs at 300 mg/kg in three female rats; neither lethality nor delayed toxicity was observed. Similarly, no behavioral changes or mortality were recorded when tested at 2500 mg×L^{-1} for 96 h as per OECD guideline 203. These findings suggest that SCSLNs are safe up to a dose of 300 mg/kg in rats and 2500 mg×L^{-1} in zebrafish.

Beam walk

When compared to the normal control group, the RT group took significantly ($p < 0.05$) more time to cross the beam, indicating effective induction of disease and reduced locomotor activity. Low mid and high doses of SCSLNs have seemed to show dose dependent improvement in time taken to cross the beam. RT + SCSLNs (60 mg × kg^{-1}) ($p < 0.01$) group had shown results comparable with that of the standard group (RT + SC (100 mg × kg^{-1}) ($p < 0.05$)) showed less activity compared to SCSLNs treated groups, as shown in Fig. 7(a).

Wire test

When compared to the healthy control group, the RT group had significantly ($p < 0.05$) lower-latency to fall. The SCSLNs treated groups exhibited a substantial improvement in grip strength. RT + SCSLNs (30 mg × kg^{-1}) ($p < 0.05$) group showed the maximum response, while the RT + SC (100 mg × kg^{-1}) ($p < 0.01$) group being the least effective among them as shown in Fig. 7(b).

Open field

The open field test was conducted to check the locomotor and exploratory behavior of the treated groups. compared to the healthy control group, the RT group had a substantial decrease in locomotor activity and exploratory behavior. The RT + SCSLNs (60 mg × kg^{-1}) ($p < 0.05$) group exhibited a substantial increase in

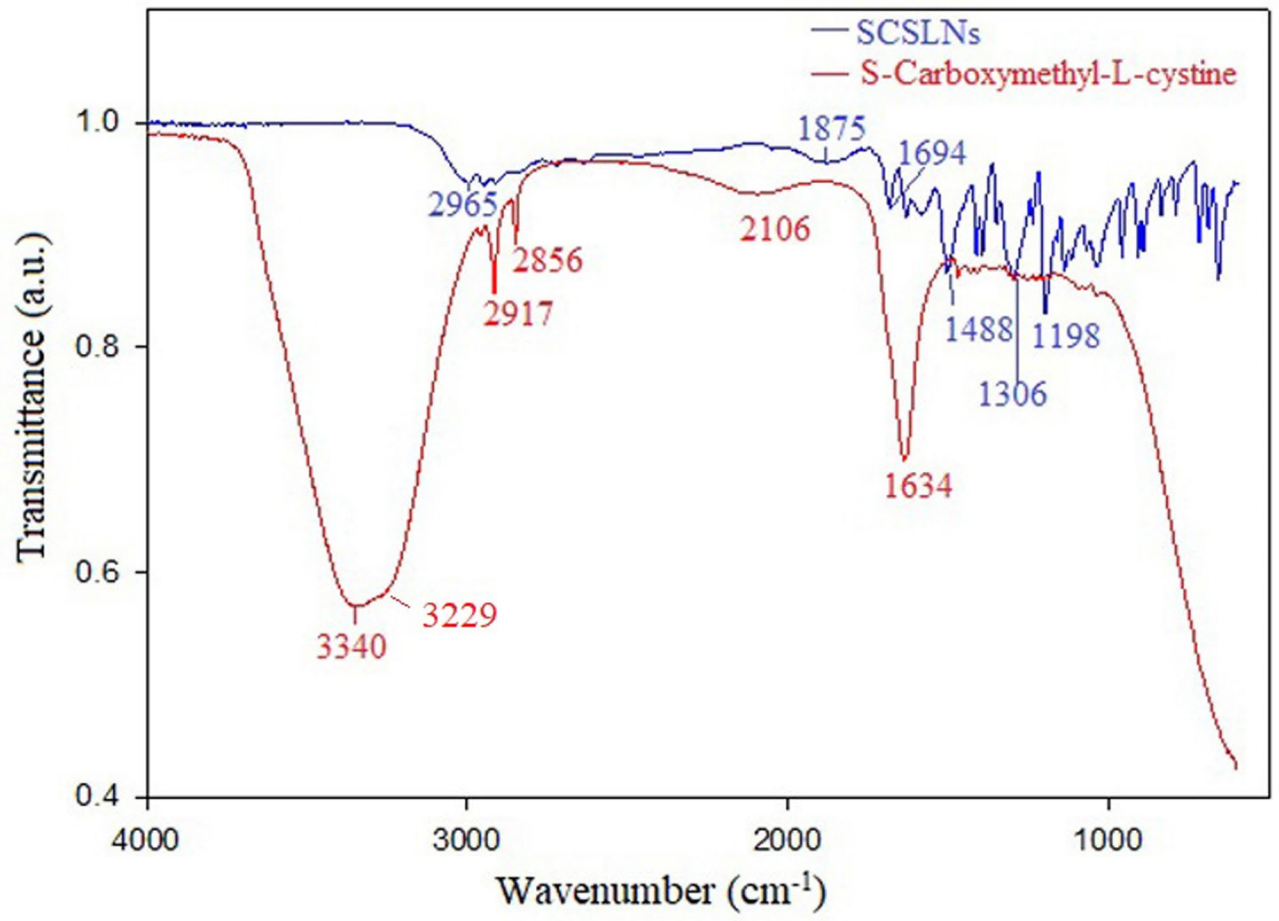

Fig. 3. FTIR spectra of SC and SCSLNs.

locomotor activity with high significance. Whereas the RT + SC (100 mg × kg^{-1}) ($p < 0.01$) group showed least locomotor activity as shown in Fig. 7(c).

Antioxidant studies: LPO, SOD, catalase, and glutathione activity

LPO, SOD, Catalase and Glutathione activity analyzed from the rat brains indicated a significant difference between the groups. LPO level was increased in the RT group rats (Fig. 7(d)), while SOD (Fig. 7(e)), Catalase (Fig. 7(f)), and Glutathione (Fig. 7(g)) levels were all decreased in the RT groups ($p < 0.05$). RT + Lev Car (10 mg × kg^{-1}) group had restored the antioxidants to a certain extent, but the RT + SCSLNs (60 mg × kg^{-1}) ($p < 0.05$) group was seen to be consistent in replenishing the antioxidants levels followed by RT + SCSLNs (30 mg × kg^{-1}), RT + SCSLNs (15 mg × kg^{-1}) and RT + SC (100 mg × kg^{-1}) groups. similar results were also seen for LPO activity.

Acetylcholine esterase Estimation

The RT group had significantly ($p < 0.05$) decreased AchE levels. RT + Lev Car (10 mg × kg^{-1}) group ($p < 0.05$) showed some increased levels compared to the RT group. Treatment of rats with high, mid, and low doses of SCSLNs significantly ($p < 0.05$ and $p < 0.01$) increased AchE activity, and with RT + SC (100 mg/kg) ($p < 0.05$) following behind as shown in Fig. 8.

Histopathology

Substantia Nigra region of control group rat brain showed normal neuronal cell morphology with no abnormalities. Substantia Nigra region of the RT group shows moderate neuronal hyperplasia, formation of LB, and gliosis. Even in the RT + Lev Car (10 mg × kg^{-1}) group moderate levels of LB are seen. In the RT + SCSLNs (15 mg × kg^{-1}) group few LB and slight gliosis can be seen. The groups treated with RT + SCSLNs (60 mg × kg^{-1}), RT + SCSLNs (30 mg × kg^{-1}), RT + SC (100 mg × kg^{-1}) showed very minute morphological changes with no abnormalities or LB as shown in Fig. 9 ((a) control; (b) RT; (c) RT + Lev Car (10 mg × kg-1); (d) RT + SC SLNs (60 mg × kg-1); (e) RT + SCSLNs (30 mg × kg-1); (f) RT + SCSLNs (15 mg × kg-1); (g) RT + SC (100 mg × kg-1)).

Distance traveled in zebrafish

The disease control groups had significantly ($p < 0.05$) traveled less distance compared to the normal control group. Treatment with RT + SCSLNs (500 µg × L^{-1}) significantly ($p < 0.01$) increased the total distance traveled

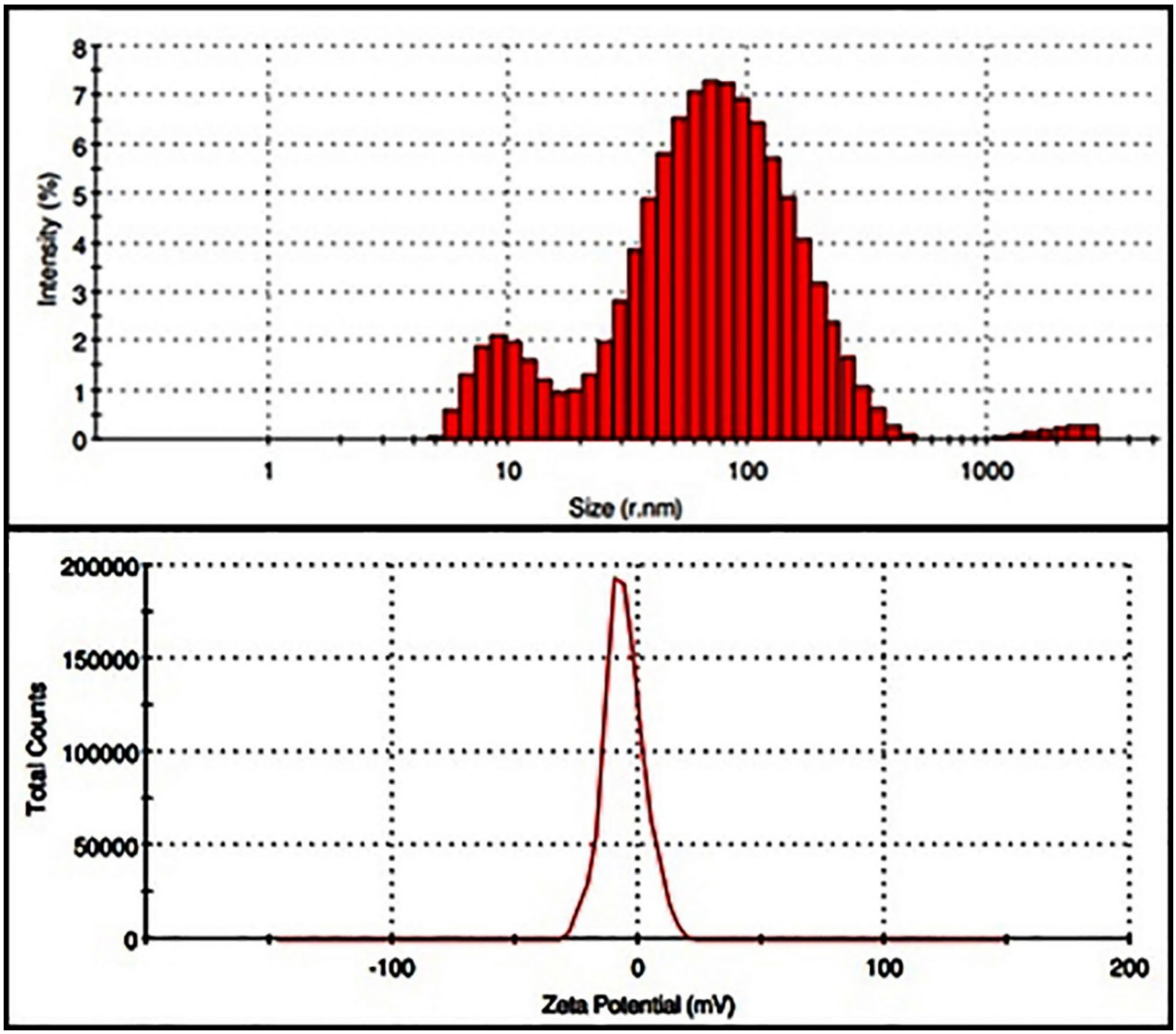

Fig. 4. The DLS measurement of the average particle size of SCSLNs (**a**) and the zeta potential of SCSLNs (**b**).

compared to disease control group. Furthermore, RT + SC (1000 µL × L^{-1}) ($p < 0.05$) had a slight increase in locomotor action, as shown in Fig. 10(a).

Acetylcholine esterase Estimation in zebrafish brain

RT treatment had drastically decreased the brain AchE levels ($p < 0.05$). Treatment with SCSLNs significantly ($p < 0.05$) restored the brain AchE levels compared to the RT treatment group. Also, in the RT + SC (1000 µL × L^{-1}) group, there was significant ($p < 0.01$) increase in AchE levels. Nevertheless, it was low compared to the formulated groups, as shown in Fig. 10(b).

Histopathology of zebrafish brain

In the control group, zebrafish corpora bigemia and cerebellum regions showed normal neuronal cell morphology with no abnormalities. Moderate neuronal hyperplasia can be seen in the RT group, and few Lewy bodies are visible. Treatment with RT + SCSLNs (500 µg × L-1), SCSLNs (250 µl×L-1), and RT + SC (1000 µL × L^{-1}) showed normal morphology, no neuronal abnormalities with slight hyperplasia, as shown in Fig. 11 ((a) group control; (b) RT; (c) RT + SCSLNs (500 µL); (d) SCSLNs (250 µL); (e) RT + SC (1000 µL)).

Discussion

PD is distinguished by the fast degeneration of DA neurons in the midbrain, followed by a gradual accumulation of Lewy bodies in the brain. The dysregulation of DA is accountable for the primary manifestations such as tremors, bradykinesia, rigidity, impaired postural reflexes, and various motor and non-motor abnormalities. Given its characteristics, PD can be classified as an irreversible, chronic, and progressive condition. Adjuvant treatment

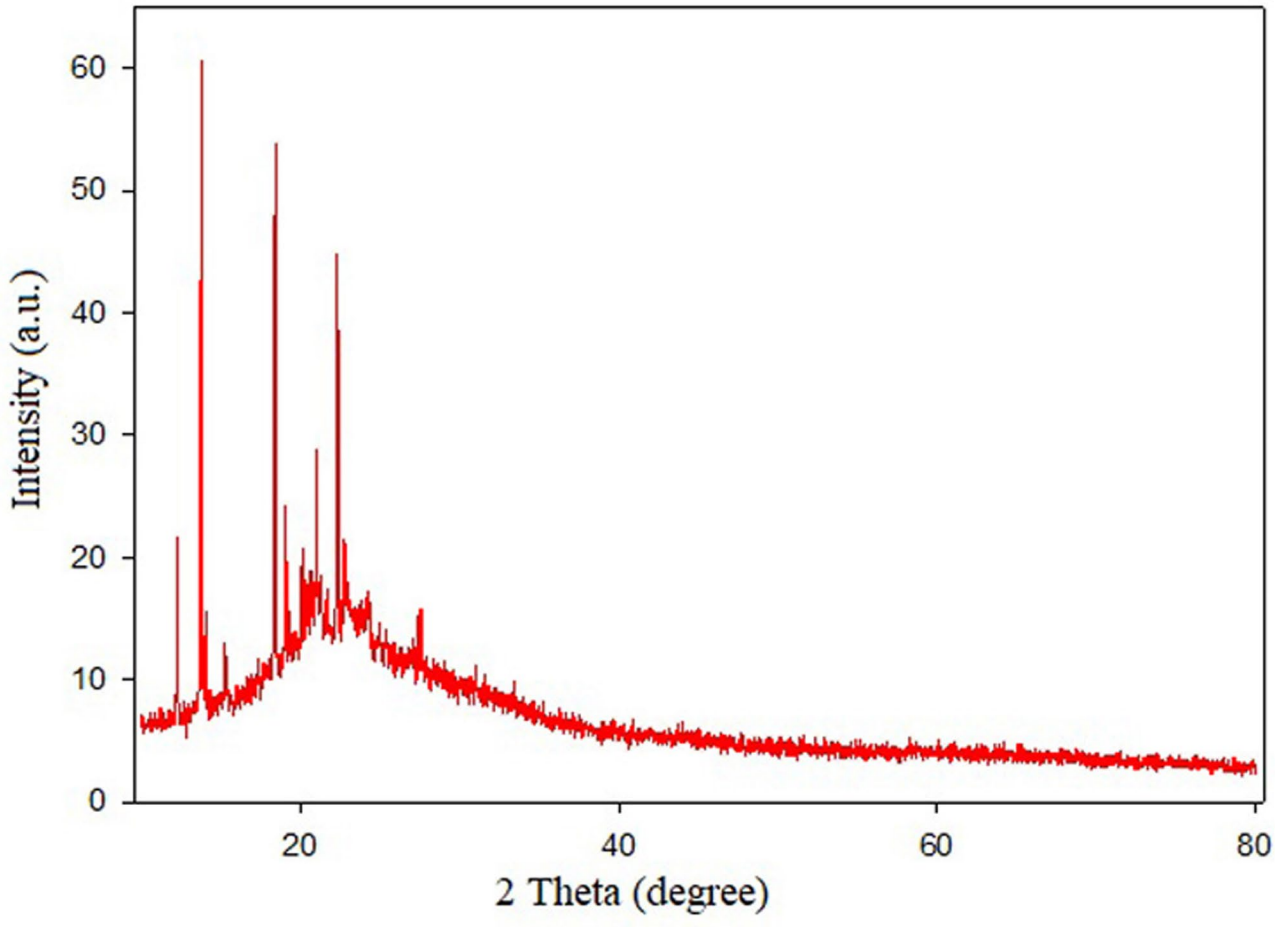

Fig. 5. XRD graph of SCSLNs.

has been suggested as a means to stabilize its progression. Several nutraceuticals have demonstrated efficacy in mitigating oxidative stress in PD[40,41]. Nevertheless, the problem of continuous and repeated administration of these nutraceuticals is required due to their short-duration action. In the case of SC, it has been reported to be slowly metabolized in patients with PD[42]. Moreover, SC has been reported to have neuroprotective action through PARK7/DJ-1, p-CREB, mBDNF, SNCA, and p-TRKb pathways in an in vitro study. Furthermore, SC has also been noted to have possible neuroprotective action by protecting the neurons from oxidative stress[43].

The present study tested the neuroprotective effect of SC-loaded SLNs on RT-induced PD in Wistar rats and zebrafish. Chronic treatment of RT has been long used in the effective induction of PD both in Rat[44–46]and zebrafish models[47–49]. RT is a type of pesticide; due to its lipophilic properties, it has a high BBB permeability. It is known to accumulate in cellular organelles; predominantly, it affects the mitochondria by binding to complex-1 and interrupts mitochondrial respiration. Furthermore, it acts by causing oxidative stress by increasing ROS production[50,51].

SLNs, pertaining to their lipophilic nature and nano-structure can easily penetrate the highly selective BBB. SLNs are further advantageous with the potential for high drug loading, easy formulation, and high stability[15]. In our study, SC-loaded SLNs were prepared by solvent evaporation-emulsification method. The resultant product was put under various physicochemical properties to confirm a successful product. After confirmation of the results, the formulation was further tested for its neuroprotective properties.

In our study, RT was administered for 28 days daily, with the treatment starting from the 14th day. Since, typically, by the time treatment for PD will be started for disease induced animals, as the disease already would have started to progress, this dosing regimen was employed. The beam walk test mainly focuses on the gait of the rat. RT treatment showed gait abnormalities, and the animal took longer to cross. Higher doses of SCSLNs showed ameliorative effects comparable to the standard drug. Similar observations were made in the animal's grip strength and explorative behavior, which were drastically affected by RT administration. However, SCSLN treatment greatly enhanced the animal's deficiencies.

In the brain, ROS is one of the key markers in dopamine metabolism, neuroinflammation, and mitochondrial dysfunction[52]. SCSLNs treatment increased SOD, Catalase, glutathione, and decreased LPO levels. This indicated that SCSLNs could effectively decrease ROS levels, indicating a pathway through which neuroprotection is achieved. Increasing data indicate decreased AchE activity in numerous brain disorders, including PD[52]. Acetylcholinesterase (AChE) is an enzyme that is very susceptible to inhibition due to the heightened production

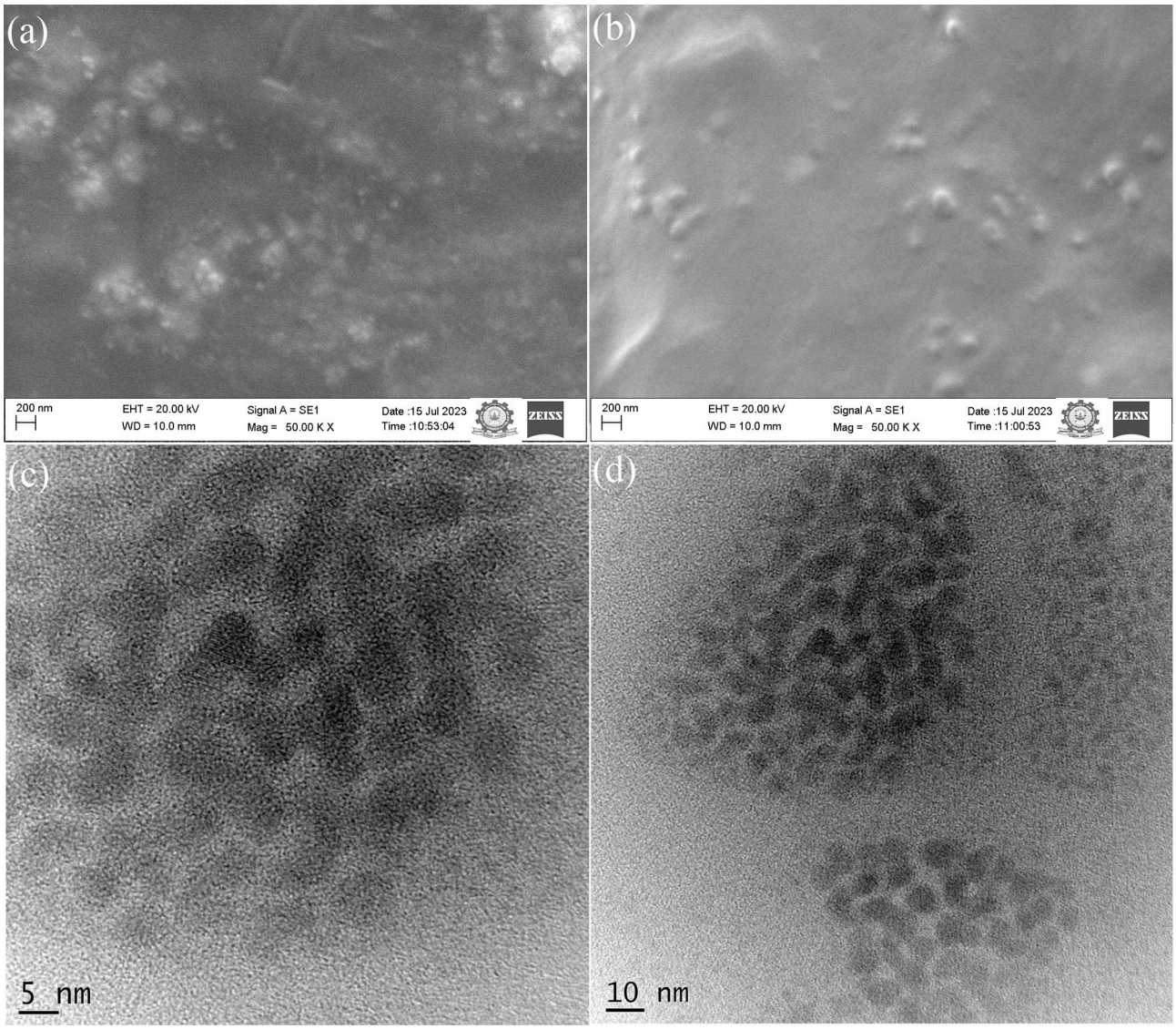

Fig. 6. SEM Images of SCSLNs(**a**) & (**b**); TEM Images of SCSLNs (**c**) & (**d**).

of radical substances. The modulation of AChE activity is a crucial therapeutic objective in the management of PD[53]. RT treatment greatly reduced AchE levels; however, the standard drug ameliorated these effects up to a certain level, but the SCSLNs treatment group had noteworthy improvement in AchE activity, with the high dose giving results close to the standard group. Chronic exposure to RT has been reported to produce LB in cells[54]. Histopathological analysis of rat SNpc region showed the mild formation of LD in the RT group. Furthermore, the standard group also was incapable of preventing the formation of LBs. However, the rest of the treatment groups were effective in completely preventing LB formation, and neuronal damage to a higher extent.

Zebrafishes are animals showing high activity and continuous lively movement with high endurance[55]. Which makes it an ideal candidate in the assessment of diseases impairing normal locomotion[56,57]. Zebrafishes exposed to RT had a drastic decrease in distance travelled. However, the SC formulation significantly restored the fish's locomotor activity. Nonetheless, the standard group was omitted from this model due to its low stability in water[58]. In the case of AchE levels, the results were highly similar to those of the rat model. Furthermore, in the histopathological analysis of the zebrafish brain, LBs were observable in the RT-exposed group with slight neuronal abnormalities. Nevertheless, no abnormalities from the normal morphology or LBs were seen in the rest of the treatment groups. The results from the rat and fish model showed little to no discrepancies.

In this study, RT treatment for 28 days successfully induced PD in rats and zebrafish. Our SCSLNs formulation showed more or less a dose-dependent action in most studies. The high-dose group has effects comparable to those of the standard groups. Although lagging in some tests, high doses showed significantly better results than those of standard groups in oxidative parameters and AchE levels. The formulation also showed promising results in brain histopathology. Furthermore, in all of the tests, SLNs loaded with SC showed superior activity compared to the unformulated drug, even though the unformulated drug was in significantly higher quantity. However, most of the tests saw a relatively consistent dose-dependent action of SCSLNs, with the unformulated

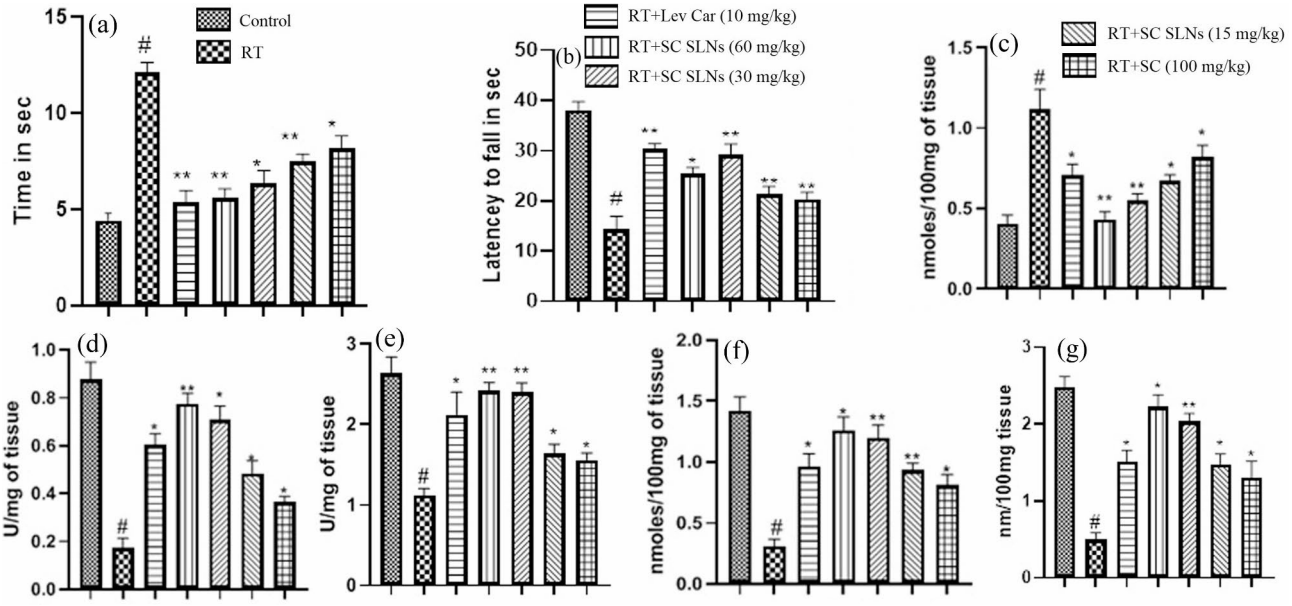

Fig. 7. Effect of SCSLNs on time taken to cross the beam (**a**), Effect of SCSLNs on latency to fall from the wire (**b**), Effect of SCSLNs on distance travelled inside the field (**c**), Graph representing the effect of SCSLNs on RT treated rat brain (**d**), MDA (**e**), SOD (**f**), catalase (**g**), and GSH levels (**h**). Each bar with a vertical line is represented as mean values ± SEM, $n = 6$. Statistical analysis was done using one-way ANOVA followed by Tukey Krammer comparison test; #$P < 0.05$, statistical significance against the control group. The *$p < 0.05$ and **$p < 0.01$ denoted statistical significance against the rotenone group.

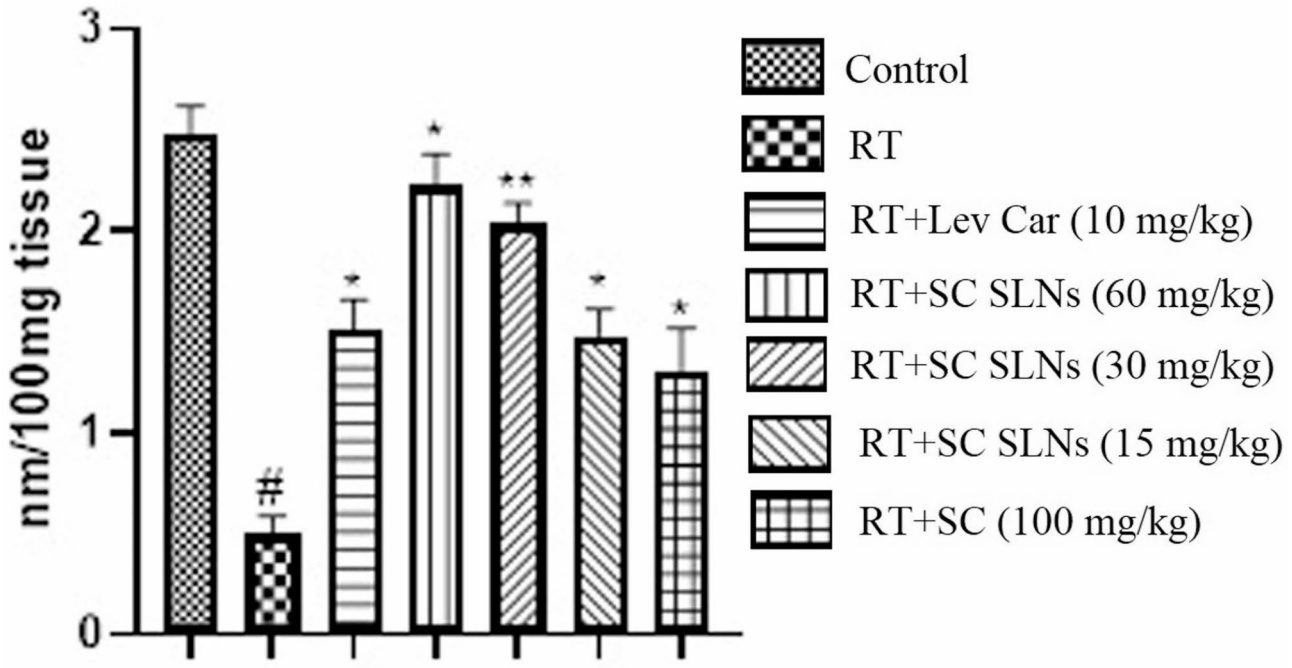

Fig. 8. Graph representing the effect of SCSLNs on Acetylcholine Esterase in rat brain. Each bar with a vertical line is defined as mean values ± SEM, $n = 6$. Statistical analysis was done using one-way ANOVA followed by Tukey Krammer comparison test; #$p < 0.05$, statistical significance against the control group. The *$p < 0.05$ and **$p < 0.01$ denoted statistical significance against the rotenone group.

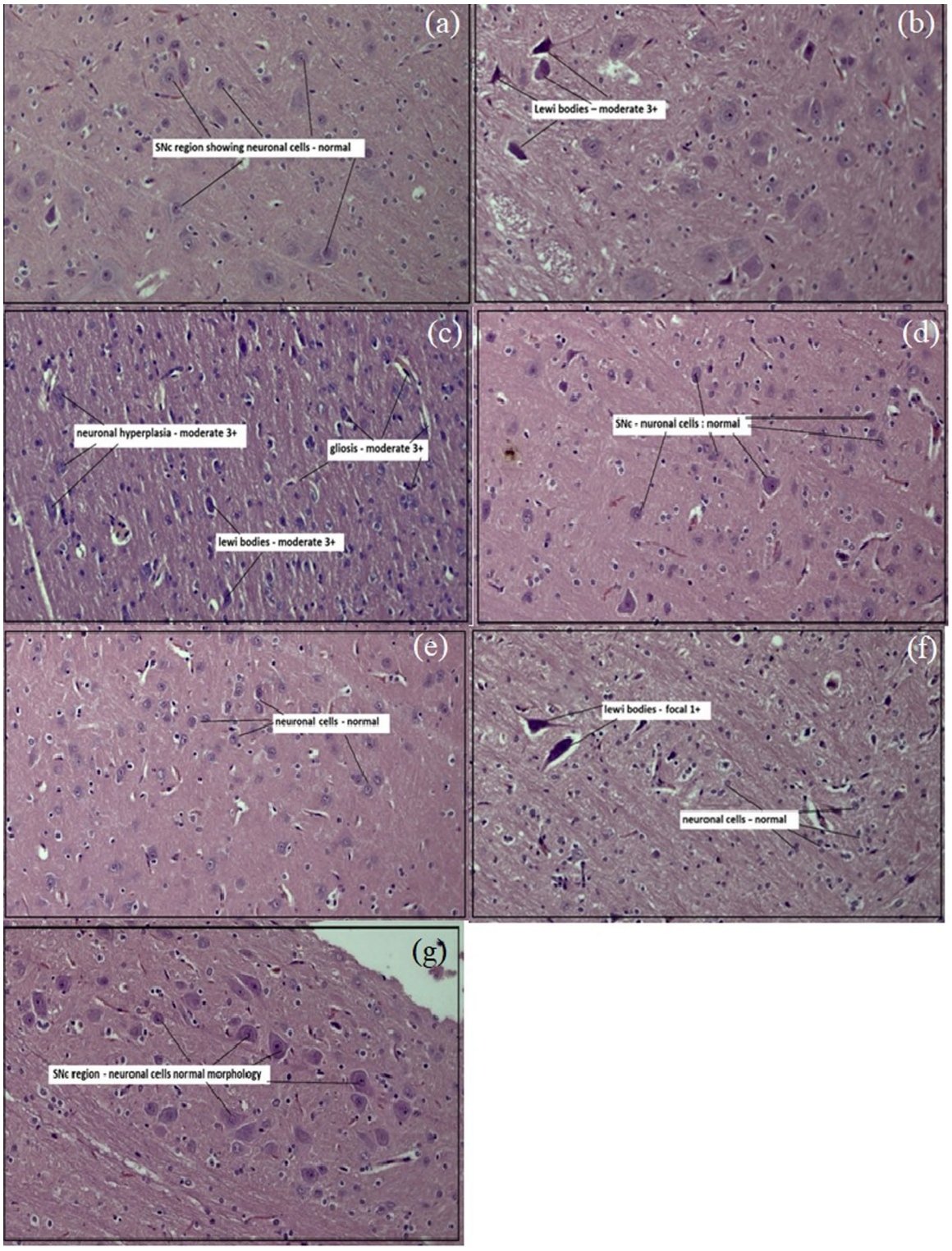

Fig. 9. Hematoxylin and eosin (H&E) stained photomicrographs of the substantia nigra from each studied group (**a**) control (**b**) RT(**c**) RT + Lev Car (10 mg × kg^{-1}) (**d**) RT + SC SLNs (60 mg × kg^{-1}) (**e**) RT + SCSLNs (30 mg × kg^{-1}) (**f**) RT + SCSLNs (15 mg × kg^{-1}) (**g**) RT + SC (100 mg × kg^{-1}).

group slightly lagging. Nevertheless, the results obtained from the rat and zebrafish models are highly consistent and co-relatable with each other. However, our study has least explored the molecular mechanism of SC. Tests on inflammatory mediators and specific PD biomarkers could be further investigated.

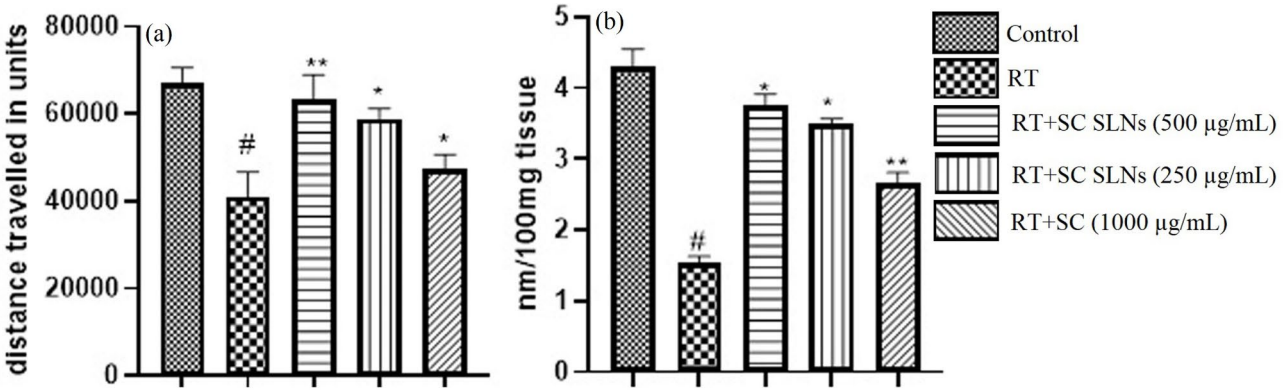

Fig. 10. Graph representing the effect of SCSLNs on distance travelled in RT-induced PD in Zebrafish (**a**) and the effect of SCSLNs on AchE in RT-induced PD Zebrafish (**b**). Each bar with a vertical line is represented as mean values ± SEM, $n = 6$. Statistical analysis was done using one-way ANOVA followed by Tukey Krammer comparison test; #$p < 0.05$, statistical significance against the control group. The *$p < 0.05$ and **$p < 0.01$ denoted statistical significance against the rotenone group.

Conclusion

The successful formulation and characterization of SC-loaded SLNs demonstrated the feasibility of using SLNs as a drug delivery system for Parkinson's treatment. The in vivo acute toxicity study of the SCSLNs demonstrated their safety profile, highlighting their potential as a viable therapeutic option for Parkinson's disease. The evaluation of the neuroprotective effect of SCSLNs on RT-induced Parkinson's in Wistar rats showed promising results, suggesting their potential for mitigating the progression of Parkinson's disease in a mammalian model. Exploring the neuroprotective potential of SCSLNs on RT-induced Parkinson's in Zebrafish provided additional evidence of their efficacy, indicating the versatility and broad applicability of the SCSLNs as a treatment option for Parkinson's disease across different animal models.

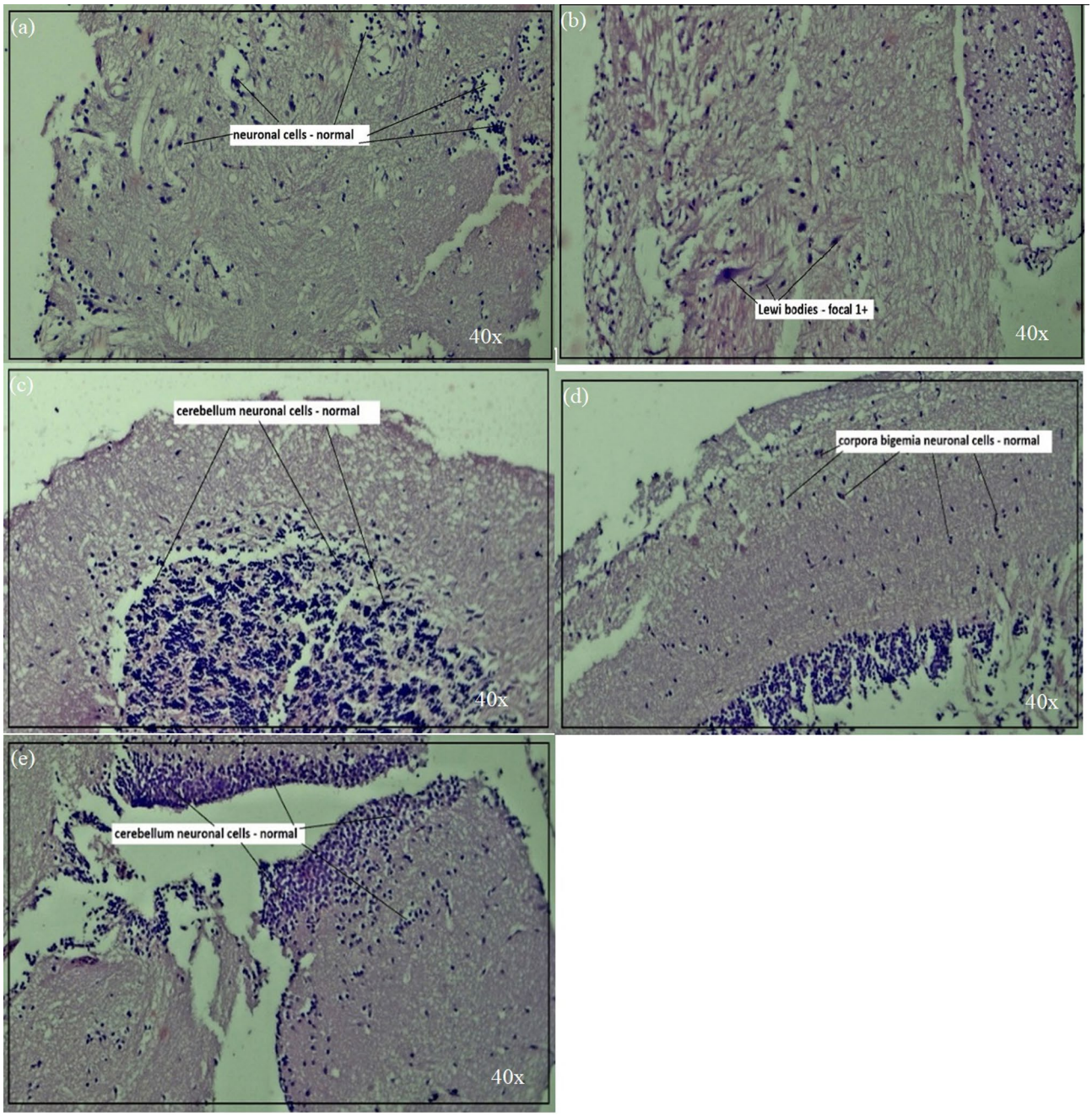

Fig. 11. Hematoxylin and eosin (H&E) stained photomicrographs of the zebrafish brain from each studied group (**a**) group control, (**b**) RT, (**c**) RT + SCSLNs (500 µL), (**d**) SCSLNs (250 µL), (**e**) RT + SC (1000 µL).

Data availability

All the data generated during the study have been included in the manuscript and supplementary files.

Received: 3 January 2025; Accepted: 24 March 2025
Published online: 29 March 2025

References

1. Feigin, V. L. et al. Global, regional, and National burden of neurological disorders, 1990–2016: a systematic analysis for the global burden of disease study 2016. *Lancet Neurol.* **18** (5), 459–480 (2019).
2. Blauwendraat, C., Nalls, M. A. & Singleton, A. B. The genetic architecture of Parkinson's disease. *Lancet Neurol.* **19** (2), 170–178 (2020).
3. Jankovic, J. Parkinson's disease: clinical features and diagnosis. *J. Neurol. Neurosurg. Psychiatry*. **79** (4), 368–376 (2008).
4. Halliday, G. M. & McCann, H. The progression of pathology in Parkinson's disease. *Ann. N. Y. Acad. Sci.* **1184** (1), 188–195 (2010).

5. Vaz, R. L., Outeiro, T. F. & Ferreira, J. J. Zebrafish as an animal model for drug discovery in Parkinson's disease and other movement disorders: a systematic review. *Front. Neurol.* **9**, 347 (2018).
6. Vijayanathan, Y. et al. 6-OHDA-lesioned adult zebrafish as a useful Parkinson's disease model for dopaminergic neuroregeneration. *Neurotox. Res.* **32**, 496–508 (2017).
7. Robea, M-A. et al. Parkinson's disease-induced zebrafish models: focussing on oxidative stress implications and sleep processes. Oxidative Medicine and Cellular Longevity. ;2020. (2020).
8. Nunes, M. E. et al. Chronic treatment with Paraquat induces brain injury, changes in the antioxidant defences system, and modulates behavioural functions in zebrafish. *Mol. Neurobiol.* **54**, 3925–3934 (2017).
9. Mitchell, S. C. & Steventon, G. B. S-carboxymethyl-L-cysteine. *Drug Metab. Rev.* **44** (2), 129–147 (2012).
10. Phillips, G. J., James, S. L. & Lethem, M. I. *Rheological properties and hydration of airway mucus. Airway Mucus: Basic Mechanisms and Clinical Perspectives* 117–147 (Springer, 1997).
11. Pedre, B., Barayeu, U., Ezeriņa, D. & Dick, T. P. The mechanism of action of N-acetylcysteine (NAC): the emerging role of H2S and sulfane sulphur species. *Pharmacol. Ther.* **228**, 107916 (2021).
12. Brandolini, L. et al. Carbocysteine lysine salt monohydrate (SCMC-LYS) is a selective scavenger of reactive oxygen intermediates (ROIs). *Eur. Cytokine Netw.* **14** (1), 20–26 (2003).
13. Pardeshi, C. et al. Solid lipid-based Nanocarriers: an overview/nanonosači Na Bazi Čvrstih lipids: pregled. *Acta Pharm.* **62** (4), 433–472 (2012).
14. Brito Raj, S., Chandrasekhar, K. B. & Reddy, K. B. Formulation, in-vitro and in-vivo Pharmacokinetic evaluation of Simvastatin nanostructured lipid carrier loaded transdermal drug delivery system. *Future J. Pharm. Sci.* **5** (1), 1–14 (2019).
15. Mehnert, W. & Mäder, K. Solid lipid nanoparticles: production, characterization and applications. *Adv. Drug Deliv. Rev.* **64**, 83–101 (2012).
16. Kaur, I. P., Bhandari, R., Bhandari, S. & Kakkar, V. Potential of solid lipid nanoparticles in brain targeting. *J. Controlled Release.* **127** (2), 97–109 (2008).
17. Safran, M. et al. GeneCards Version 3: the human gene integrator. Database. ;2010. (2010).
18. Huang, B., Xiong, J., Zhao, X., Zheng, Y. & Zhu, N. Network pharmacology-based analysis of the pharmacological mechanisms of aloperine on cardiovascular disease. Evidence-Based Complementary and Alternative Medicine. ;2020. (2020).
19. Raudvere, U. et al. G: profiler: a web server for functional enrichment analysis and conversions of gene lists (2019 update). *Nucleic Acids Res.* **47** (W1), W191–W8 (2019).
20. Ge, S. X., Jung, D. & Yao, R. ShinyGO: a graphical gene-set enrichment tool for animals and plants. *Bioinformatics* **36** (8), 2628–2629 (2020).
21. Jia, A., Xu, L. & Wang, Y. Venn diagrams in bioinformatics. *Brief. Bioinform.* **22** (5), bbab108 (2021).
22. Panneerselvam, T. et al. *Graph Theoretical analysis, in silico modelling and molecular dynamic studies of (5-((2-chloropyridin-4-yl) oxy)-3-phenyl-1H-pyrazol-1-yl)-2-(4-substituted phenyl)-N, N-dimethylethen-1-amine derivatives for the treatment of breast cancer* (Anti-cancer Agents in Medicinal Chemistry, 2022).
23. Kalimuthu, A. K. et al. Pharmacoinformatics-based investigation of bioactive compounds of Rasam (South Indian recipe) against human cancer. *Sci. Rep.* **11** (1), 21488 (2021).
24. Kunjiappan, S. et al. Design, graph theoretical analysis and in Silico modelling of Dunaliella Bardawil biomass encapsulated keratin nanoparticles: a scaffold for effective glucose utilization. *Biomed. Mater.* **13** (4), 045012 (2018).
25. Asasutjarit, R. et al. Effect of solid lipid nanoparticles formulation compositions on their size, zeta potential and potential for in vitro pHIS-HIV-hugag transfection. *Pharm. Res.* **24**, 1098–1107 (2007).
26. Abdelbary, G. & Fahmy, R. H. Diazepam-loaded solid lipid nanoparticles: design and characterization. *Aaps Pharmscitech.* **10**, 211–219 (2009).
27. Kumar, R. et al. Preparation, characterization and vitro cytotoxicity of Fenofibrate and Nabumetone loaded solid lipid nanoparticles—Materials. *Sci. Engineering: C.* **106**, 110184 (2020).
28. OECD. *Test no. 420: acute oral toxicity—fixed dose procedure* (Organization for Economic Co-Operation and Development Paris, France, 2002).
29. No, O. T. 203: Fish, acute toxicity test. OECD guidelines for the testing of chemicals, Section. ;2:02–24. (1992).
30. Chen, S. F., Hsu, C. W., Huang, W. H. & Wang, J. Y. Post-injury Baicalein improves histological and functional outcomes and reduces inflammatory cytokines after experimental traumatic brain injury. *Br. J. Pharmacol.* **155** (8), 1279–1296 (2008).
31. Hadadianpour, Z. et al. The effect of orexin-A on motor and cognitive functions in a rat model of Parkinson's disease. *Neurol. Res.* **39** (9), 845–851 (2017).
32. Kuniishi, H. et al. Early deprivation increases high-leaning behavior, a novel anxiety-like behavior, in the open field test in rats. *Neurosci. Res.* **123**, 27–35 (2017).
33. Ohkawa, H., Ohishi, N. & Yagi, K. Assay for lipid peroxides in animal tissues by thiobarbituric acid reaction. *Anal. Biochem.* **95** (2), 351–358 (1979).
34. Aebi, H. *Catalase. Methods of enzymatic analysis* 673–684 (Elsevier, 1974).
35. Fishman, W. H. *Metabolic Conjugation and Metabolic Hydrolysis: Volume I* (Academic, 2014).
36. Misra, H. P. & Fridovich, I. The oxidation of phenylhydrazine: superoxide and mechanism. *Biochemistry* **15** (3), 681–687 (1976).
37. Ellman, G. L., Courtney, K. D., Andres, V. Jr & Featherstone, R. M. A new and rapid colorimetric determination of acetylcholinesterase activity. *Biochem. Pharmacol.* **7** (2), 88–95 (1961).
38. Audira, G. et al. A simple setup to perform 3D locomotion tracking in zebrafish by using a single camera. *Inventions* **3** (1), 11 (2018).
39. Azevedo, R. D. et al. Effects of Pyriproxyfen on zebrafish brain mitochondria and acetylcholinesterase. *Chemosphere* **263**, 128029 (2021).
40. Wang, Y., Chen, Y., Zhang, X., Lu, Y. & Chen, H. New insights in intestinal oxidative stress damage and the health intervention effects of nutrients: A review. *J. Funct. Foods.* **75**, 104248 (2020).
41. Benot-Dominguez, R. et al. Olive leaf extract impairs mitochondria by pro-oxidant activity in MDA-MB-231 and OVCAR-3 cancer cells. *Biomed. Pharmacother.* **134**, 111139 (2021).
42. McFadden, S. A. Phenotypic variation in xenobiotic metabolism and adverse environmental response: focus on sulfur-dependent detoxification pathways. *Toxicology* **111** (1–3), 43–65 (1996).
43. Catanesi, M. et al. S-Carboxymethyl cysteine protects against oxidative stress and mitochondrial impairment in a Parkinson's disease in vitro model. *Biomedicines* **9** (10), 1467 (2021).
44. Wang, S. et al. Effect of moxibustion on mTOR-mediated autophagy in rotenone-induced Parkinson's disease model rats. *Neural Regeneration Res.* **13** (1), 112 (2018).
45. Michel, H. E., Tadros, M. G., Esmat, A., Khalifa, A. E. & Abdel-Tawab, A. M. Tetramethylpyrazine ameliorates rotenone-induced Parkinson's disease in rats: involvement of its anti-inflammatory and anti-apoptotic actions. *Mol. Neurobiol.* **54**, 4866–4878 (2017).
46. Sharma, S., Kumar, P. & Deshmukh, R. Neuroprotective potential of spermidine against rotenone-induced Parkinson's disease in rats. *Neurochem. Int.* **116**, 104–111 (2018).
47. Ünal, İ. et al. Neuroprotective effects of mitoquinone and Oleandrin on Parkinson's disease model in zebrafish. *Int. J. Neurosci.* **130** (6), 574–582 (2020).
48. Hettiarachchi, P., Niyangoda, S. S., Jarosova, R. & Johnson, M. A. Dopamine release impairments accompany locomotor and cognitive deficiencies in Rotenone-Treated Parkinson's disease model zebrafish. *Chem. Res. Toxicol.* **35** (11), 1974–1982 (2022).

49. Ma'arif, B. et al. The effect of ethanol extract of Marsilea crenata Presl. Leaves on rotenone-induced zebrafish locomotor activity. *Jurnal Farmasi Sains Dan. Komunitas (JFSK)*. **19** (2), 87–92 (2022).
50. Wang, Y. et al. Parkinson's disease-like motor and non-motor symptoms in rotenone-treated zebrafish. *Neurotoxicology* **58**, 103–109 (2017).
51. Ünal, İ. & Emekli-Alturfan, E. Fishing for Parkinson's disease: A review of the literature. *J. Clin. Neurosci.* **62**, 1–6 (2019).
52. Dias, V., Junn, E. & Mouradian, M. M. The role of oxidative stress in Parkinson's disease. *J. Parkinson's Disease*. **3** (4), 461–491 (2013).
53. Hasan, W., Kori, R. K., Jain, J., Yadav, R. S. & Jat, D. Neuroprotective effects of mitochondria-targeted Curcumin against rotenone-induced oxidative damage in the cerebellum of mice. *J. Biochem. Mol. Toxicol.* **34** (1), e22416 (2020).
54. Borland, M. K. et al. Chronic, low-dose rotenone reproduces lewy neurites found in the early stages of Parkinson's disease, reduces mitochondrial movement and slowly kills differentiated SH-SY5Y neural cells. *Mol. Neurodegeneration*. **3** (1), 1–12 (2008).
55. Burris, B., Jensen, N. & Mokalled, M. H. Assessment of swim endurance and swim behavior in adult zebrafish. *JoVE (Journal Visualized Experiments)*. **177**, e63240 (2021).
56. Flinn, L., Bretaud, S., Lo, C., Ingham, P. W. & Bandmann, O. Zebrafish as a new animal model for movement disorders. *J. Neurochem.* **106** (5), 1991–1997 (2008).
57. Razali, K. et al. The promise of the zebrafish model for Parkinson's disease: today's science and tomorrow's treatment. *Front. Genet.* **12**, 655550 (2021).
58. Pappert, E. J. et al. Levodopa stability in solution: time course, environmental effects, and practical recommendations for clinical use. *Mov. Disorders: Official J. Mov. Disorder Soc.* **11** (1), 24–26 (1996).

Acknowledgements

The authors thank M.S. Ramaiah University of Applied Sciences and Chromed Biosciences Pvt. Ltd. for supporting this project by providing the necessary facilities. The authors extend their appreciation to the Deanship of Scientific Research at King Khalid University for funding this work through a Large Group Research Project under grant number RGP.2/83/45.

Author contributions

SDA, SHR, GKR, GS, SK, DNA and PP conceived and designed the research. SDA, SHR, GKR, GS, SR, SN, PT, BSK, SK, DNA and PP conducted the experiments. SDA, SHR, GKR, GS, BGHD, SG, SK, DNA and PP analyzed the data. SDA, SHR, GKR, GS, SK, KC, DNA and PP wrote the manuscript. All authors read and approved the manuscript.

Funding

No external funding was received.

Declarations

Competing interests

The authors declare no competing interests.

Ethics approval and consent to participate

All experimental animal procedures were performed after obtaining prior approval from the Institutional Animal Ethical Committee (IAEC Ref No.: XXVII/MSRFPH/COL/PG-05/13.02.2023).

Additional information

Supplementary Information The online version contains supplementary material available at https://doi.org/10.1038/s41598-025-95806-0.

Correspondence and requests for materials should be addressed to S.K., D.N.A. or P.P.